On the Multi-Factor State-Space Modelling of European Union Allowance Futures Prices

By

Jun Seok Han

A thesis submitted to Macquarie University

for the degree of Master of Research

Department of Mathematics and Statistics

February 2021

MACQUARIE
University
SYDNEY·AUSTRALIA

Examiner's Copy

Typeset in LaTeX 2_ε.

Except where acknowledged in the customary manner, the material presented in this thesis is, to the best of my knowledge, original and has not been submitted in whole or part for a degree in any university.

Jun Seok Han

Acknowledgements

First and foremost, I would like to express my sincere gratitude to my principal supervisor, Dr. Nino Kordzakhia, for her continuous support, encouragement and patience throughout the course of my research project. Her expertise, guidance, criticism, and passion have enormously assisted me in discovering new areas in the discipline of statistics and quantitative finance, and led me to build confidence in statistics research. I would also like to express appreciation to my associate supervisor, Prof. Pavel Shevchenko, for his invaluable advice and insightful comments throughout the year.

Special thanks to the Department of Mathematics and Statistics, Macquarie University, and Macquarie Business School, for providing such a wonderful experience and a pleasant working environment for my research project.

Lastly, I am eternally grateful to my parents in Korea, for their endless love and faith in me. Their continuous support and encouragement have let me grow and study in a better environment. I also would like to thank my aunt, her family, and my friends, both in Korea and in Sydney, for their enormous support all the time.

Abstract

To confront rising greenhouse gas emissions, the European Union Emissions Trading System (EU ETS) was introduced in 2005. The EU ETS covers all major CO_2 emitting industries, and next to European Union Allowance (EUA) spot contracts, there is also a wide range of futures contracts available for trading. This study presents a new multi-factor state-space model for risk-neutral pricing of EUA futures that can also be applied for out-of-sample estimation of futures prices. A comparative analysis of the performance of this state-space model with correlated measurement errors versus reduced-form models is conducted. The Kalman filtering technique is used for the estimation of the state variables, subsequently estimating the model parameters by maximising a marginal likelihood function. We illustrate the proposed model, using a cross-section of daily futures contracts for the sample period from January 2016 - August 2020 that corresponds to the Phase III period of the EU ETS.

Contents

List of Figures

List of Tables

1

Introduction

1.1 Background and Aims

In pricing theory, it is assumed that pricing of commodity derivatives is developed under the risk-neutral framework. Black [9] first developed the risk-neutral pricing theory for commodity derivatives in the Black-Scholes-Merton framework, in Black and Scholes [10] and Merton [32], where a single factor, being the commodity spot price, is represented as a Geometric Brownian Motion (GBM). The principles of Black-Scholes-Merton's framework laid foundation for asset pricing theory. Since then, many models were developed by considering a number of factors as stochastic processes, which reflect the specifics of the commodity market. The mean-reverting process, or the Ornstein-Uhlenbeck (O-U) process is commonly used to model the dynamics of commodities or their derivative prices. For example, in the two-factor oil contingent claims pricing model in Gibson and Schwartz [23], a mean-reverting factor and GBM were employed for modelling of the convenience yield and correlated oil spot price, respectively.

One of the widely used existing models for pricing of commodities is the Schwartz-Smith two-factor model in Schwartz and Smith [37]. In this model, the spot price of a commodity is defined as the sum of two factors, so-called short-term deviations and long-term equilibrium price level. The short-term factor is assumed to tend to zero, as it stems from the idea that it reflects short-term variations in prices due to temporary changes in demand, supply, and current market conditions, which will be corrected as the market responds over time. The long-term factor is assumed to follow a Brownian motion with drift, which reflects expected permanent changes in equilibrium price level, according to the advancement in technology for production, or any political and regulatory changes.

The Schwartz-Smith two-factor model is interpreted as a linear state-space model. This setup is widely used in mathematical finance and econometrics for pricing of derivatives and making predictions of prices of different types of commodities using the component latent factors. Conceptually, as these latent factors are not directly observable, the Kalman filter is implemented to estimate latent variables, and parameters are estimated by maximising the marginal likelihood function. The Kalman smoother is also used to estimate state variables based on filtered values, which is conceptually used for making predictions within the same period considered for estimation.

In this thesis, we compare different reduced-form models, based on the Schwartz-Smith two-factor model, with seasonal component as a deterministic factor. The novelty of our approach consists in the implementation of correlations of measurement errors between contracts of various maturities, which were assumed to be zero in the original model. Hence, we allow measurement errors to be correlated with each other, and estimate not only the model parameters, but also the correlation matrix of measurement errors in the model. We also present the method of estimating volatilities of measurement errors based on a parametric function in terms of maturities. For illustration, we use the historical daily EUA futures prices, obtained by Macquarie University access to Refinitiv Datascope, and compare performances of different reduced-form models. Models used in the comparative analysis are:

Model 1: A single-state variable which follows the Brownian motion;

Model 2: The classical Schwartz-Smith two-factor model;

Model 3: Two state variables which follow the Ornstein-Uhlenbeck processes;

Model 4: Model 3 with correlated measurement errors; and

Model 5: Model 4 with volatilities of measurement errors defined in a parametric form.

1.2 European Union Allowance Market

The United Nations Framework Convention on Climate Change (UNFCCC) is the key international organisation which initially aimed at preventing climate change by legally binding emission reduction targets to nations listed in Annex I of UNFCCC [42]. The annually held conferences have naturally led to the Kyoto Protocol, which was adapted in December 1997, for negotiations on emission targets, commitment periods and legally binding obligations between groups of industrialised countries, Occhipinti and Verona [34]. As a result, the European Union Emission Trading System (EU-ETS) was launched in 2005, with its aim to reduce greenhouse gas (GHG) emissions from a variety of different sectors, such as agriculture, aviation, energy, and manufacturing industries across Member States. The implementation of the system puts obligations on those sectors to surrender one unit of European Union Allowance (EUA) in order to emit one tonne of CO_2 or equivalent gases as defined initially in Protocol [43], and updated in Doha Amendment [19]. Otherwise, they face a serious financial penalty, which is set to be paid per tonne of pollutant that does not offset by EUAs held at the end of a pre-determined period.

As the U.S. Acid Rain Program that launched in 1995 has been evaluated as one of a successful policy in mitigating the overall atmospheric levels of SO_2, Napolitano et al. [33], the notion of the cap-and-trade scheme is considered as one of the most trustworthy and feasible mechanism. This scheme was expected to effectively reduce levels of GHG emissions. As per the Protocol in [43], during Phase I (2005-2007) and Phase II (2008-2012) of the EU-ETS, allocation of emission allowances were established by each Member State's National Allocation Plan, and approximately 90% and more of free allowances were allocated to sectors committed to compliance. Currently in Phase III (2013-2020), which was agreed after Doha Amendment [19] in December 2012, 57% of allowances were allocated to be auctioned, with the remaining allowances being allocated through the National Allocation Plan. Lastly in Phase IV (2021-2030), the allocation rules will be revised for effectiveness and efficiency of the distribution of the declining amount of free allowances. Emission reduction targets were also revised after Paris Agreement in 2015, to contribute towards preventing the threat of climate change by holding the increase of global temperature below 2° C, as reported by UNFCCC in [44].

Since the opening of the EUA market, futures trading has been very active. Brokers began facilitating trades between market participants, and as trading prices have been tracked

and recorded, the market constantly developed with an increase in transactions managed by more intermediaries, Convery and Redmond [14]. Such financial derivatives have been very attractive, as they allow entities to hedge against potential financial risks, such as uncertainty in prices of EUA in upcoming future due to fluctuations in energy demand, or changes in production figures, Trück and Weron [41].

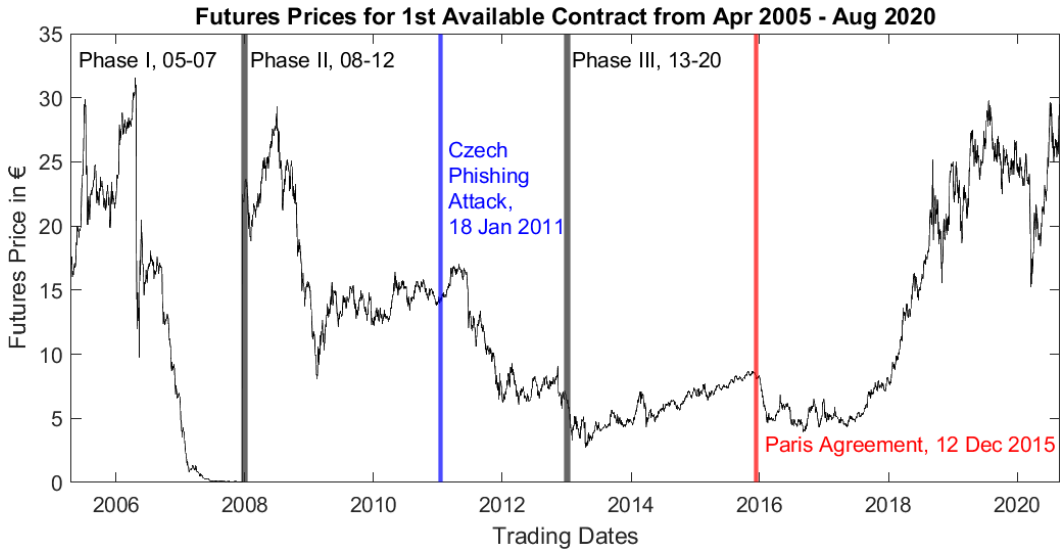

Figure 1.1: Path of prices of first available EUA futures contract for the period from April 22, 2005 to August 31, 2020. Black lines represent when each subsequent phase began; Blue line shows when the Czech emission registry was attacked in 2011; Red line shows the end date of the Paris Agreement meeting in 2015.

Figure 1.1 depicts the time series plot of first available EUA futures prices, traded in the Intercontinental Exchange. Towards the end of Phase I, futures prices were almost at zero, due to excessive proportion of free allowances allocated to companies. As Phase II of the EU-ETS began in 2008, with changes in regulations as per amendment in [19], futures contracts continued trading at a reasonable price level, similar to the beginning of Phase I. However, in January 2011, there was a serious cyberattack to the managing company of the Czech Republic's emissions registry, which had a financial damage of €7 million, which was equivalent to 500,000 EUAs at a price of €14, Ainsworth [2]. On top of that, the price level began to decrease from 2011, remaining at a lower level until 2017. Studies prior to 2011 viewed that the carbon price will increase up to €40 based on the European Commission's aim to reduce GHG emission by 20% below 1990 level, and began proposing appropriate policies for the trading system, Delbeke et al. [18]. Edenhofer [20] argued that

reforms in the EU-ETS were required, as the futures price level between €5 and €6 was at an insufficient level to encourage businesses to develop eco-friendly alternative technologies. The EU-ETS was reformed in 2018, where the linear reduction factor of the cap of GHG emission level increased from 1.74% to 2.2% per year. However, Flachsland et al. [21] was still concerned with the design of the EU-ETS and argued that a price floor will contribute to improvement in the EU-ETS, by reducing the risk of a dynamically inefficient price formation. For further description on the EU-ETS, readers are referred to the official website: European Commission: EU Emissions Trading System[1].

1.3 Literature Review

The EUA market has a relatively short history, compared to other commodities such as crude oil. Nonetheless, proactive studies have been performed within the last decade in the analysis of the EU-ETS, modelling of EUA futures contracts, and options on futures contracts. Based on the characteristics of EUA in the first year since opening of the market, Benz and Trück [4] suggested that in the long term, the mean-reversion feature may be motivated by the policy and regulatory issues, and the market fundamentals that affect the demand and supply of EUA will yield short-term price or volatility shocks. For Phase I of the EU-ETS, Seifert et al. [38] found that EUA prices do not need to follow any seasonal patterns, and the martingale property is valid on the discounted prices of EUA. Abadie and Chamorro [1] used a single-factor GBM model and set up a linear state-space model to estimate futures prices over Phase I using the Kalman filter, where the spot price of EUA was considered as a latent variable. Benz and Trück [5] used Markov-switching and AR-GARCH models for stochastic modelling, whereas Daskalakis et al. [17] allowed for stochastic jumps in modelling of spot prices of EUA, and used the cost-of-carry relationship to define prices of futures contracts. However, Trück and Weron [41] showed that based on the price during Phase II and the first half of Phase III, futures contracts were priced at a significantly higher level than the price implied by the cost-of-carry relationship. Carmona and Hinz [11] took a different approach, considering the non-compliance event in terms of the total normalised emission, along with the level of penalty. They used the digital nature of the terminal allowance price as the basis for modelling of the spot price process, and hence pricing of European options on

[1]European Commission: EU Emissions Trading System, https://ec.europa.eu/clima/policies/ets_en

EUA futures. This reduced-form model was evaluated by Hitzemann and Uhrig-Homburg [28], for which they extended the two-period market model and considered using different model variants for different compliance periods during Phase II of the EU-ETS. In the EUA pricing model established by Carmona and Hinz [11], Wen and Kiesel [46] developed a bivariate model in state-space form for parameter estimation through the Kalman filter, using December-maturity futures contracts from 2005 to 2012. Recently, Aspinall et al. [3] has evaluated the term structure of EUA futures prices and compared performances of a single-factor GBM model by Abadie and Chamorro [1] and the classic Schwartz-Smith two-factor model by Schwartz and Smith [37].

Also reviewing models for pricing of commodities other than EUA, Cortazar et al. [15] proposed a multicommodity model which dynamics of state variables follow the Ornstein-Uhlenbeck process, and Binkowski et al. [8] extended the study for pricing of crude oil futures contracts, modifying the two-factor model in Schwartz and Smith [37] to allow the long-term factor to follow a mean-reverting process. Further, the parameter identification problem for the two-factor model in this setup has been studied in Binkowski et al. [7] to improve the performance of estimation. Cortazar et al. [16] incorporated both futures prices and analysts' spot price forecasts in the Kalman filter to evaluate the term structure in the crude oil market, and Cifuentes et al. [13] extended the analysis in the copper market. A novel method for testing the predictability of futures prices was proposed by Kuruppuarachchi et al. [31], where the Kalman filter procedure has been modified to incorporate heteroscedasticity of prices and to estimate time-varying risk premium. For pricing of agricultural commodities, Sørensen [40] studied the performance of Schwartz-Smith two-factor model, using Fourier series as a seasonal component. An attempt at estimating covariances of measurement errors was also made, using a parametrised function of the time to maturity, but claimed that a substantial improvement in the model could not be seen. Geman and Nguyen [22] allowed the deterministic seasonal component in the volatility of latent factors and used a function of inverse inventory as the third state variable in the model. A step function was used in Peters et al. [35] as a seasonal component for calibration of commodity spot and futures prices in a general multi-factor model, and a multi-factor model of commodity futures has been developed with stochastic seasonality in Hevia et al. [27]. Under the same setup as in Schwartz and Smith [37] and Sørensen [40], instead of optimising the sample likelihood function, Guo [25] proposed a different estimation method, so-called a two-step least-square

estimation method, which involves minimising the sum of squared residuals from the state equation.

1.4 Computation Environment

The software used for this project was MATLAB R2020b. The required computations for parameter estimations and analyses in EUA futures price data were done using computers with 4 vCPUs and 64GB RAM. For each model presented in Chapter 3 of this thesis, the computation time taken was approximately 5 days. Codes for a simulation study are accessible here[2].

1.5 Outline of the Thesis

The remaining sections of this thesis are organised as follows. In Chapter 2, we introduce pricing models for comparison, along with detailed steps of the Kalman filter and smoothing algorithm for estimation of state variables, and subsequently for parameter estimation for Models 1-5 described in Section 1.1. In Chapter 3, we illustrate the calibration to the real data using historical daily EUA futures prices and compare performances of reduced-form models. Chapter 4 concludes with overall discussion of this project, with proposals of possible future works to further extend this study. Appendix A shows the derivation of expectation and variance of latent variables, and hence, the derivation of futures prices. Appendix B shows the MATLAB code which can be used for a simulation study.

[2]Codes are available at https://github.com/Junee1992/EUA_Futures_Pricing

2

Pricing Models

2.1 The Extended Schwartz-Smith Two Factor Model

In this section, we present the modified version of the Schwartz-Smith two-factor model, Schwartz and Smith [37].

2.1.1 Modelling the Spot Price

We define two latent variables χ_t and ξ_t to be the short-term deviations and the long-term equilibrium price level, and define $g(t)$ to be the seasonal component. Suppose S_t is the spot price of a commodity at time t. Then, the logarithm of the spot price is defined as

$$\ln S_t = \chi_t + \xi_t + g(t). \tag{2.1}$$

Following the idea from Binkowski et al. [8], in the extended Schwartz-Smith two-factor model we assume that χ_t are short-term effects which revert towards zero, and ξ_t are also following the O-U process, reverting towards the long-term mean level μ_ξ. Dynamics of two

latent variables are expressed in terms of stochastic differential equations as

$$d\chi_t = -\kappa\chi_t dt + \sigma_\chi dW_t^\chi, \tag{2.2}$$

$$d\xi_t = (\mu_\xi - \gamma\xi_t)dt + \sigma_\xi dW_t^\xi, \tag{2.3}$$

where $\kappa, \gamma > 0$ are the speed of the mean-reversion for χ_t and ξ_t, respectively, and $\sigma_\chi, \sigma_\xi > 0$ are instantaneous volatilities of two latent variables. W_t^χ and W_t^ξ are correlated standard Brownian processes, and $\mathbb{E}\left[dW_t^\chi dW_t^\xi\right] = \rho_{\chi\xi}dt$, where $\rho_{\chi\xi}$ is the correlation coefficient of two stochastic processes.

It is quite evident that futures prices, especially in energy and agricultural commodities, fluctuate with some seasonal pattern. The seasonal component $g(t)$ can be considered directly in the price, or it can be taken into account in price volatilities. Depending on the empirical evidence of the price data, the seasonal component can be deterministic or stochastic. Considering the deterministic seasonality, $g(t)$ is expressed as some function of time t. Typically, types of seasonal component include a step-wise function, for which different constant values are added to price at each sub-period, or it is expressed as some pre-determined parametric function. In this thesis, we study the cyclic pattern of the price as the sum of sinusoidal functions. Note that the linear trend is also considered in $g(t)$. The seasonal effect $g(t)$ of the spot price of a commodity at time t, is expressed as

$$g(t) = \alpha + \delta t + \sum_{h=1}^{q}\left[a_h \cos\left(\frac{2\pi t}{A_h}\right) + b_h \sin\left(\frac{2\pi t}{A_h}\right)\right], \tag{2.4}$$

where α is the intercept of the trend, δ is the linear trend of the spot price, q is the number of harmonics, A_h are periodicities for each harmonic in terms of days, where $h = 1, ..., q$.

Based on two stochastic processes in (2.2) and (2.3), the distribution of the logarithm of the spot price, along with the expectation and the variance, can be expressed in a closed form. As (2.2) and (2.3) indicate that χ_t and ξ_t are jointly normally distributed, their expectations and variances are derived as

$$\mathbb{E}[(\chi_t, \xi_t)] = \left(e^{-\kappa t}\chi_0, \frac{\mu_\xi}{\gamma}\left(1 - e^{-\gamma t}\right) + e^{-\gamma t}\xi_0\right), \tag{2.5}$$

$$Cov[(\chi_t, \xi_t)] = \begin{pmatrix} \frac{1-e^{-2\kappa t}}{2\kappa}\sigma_\chi^2 & \frac{1-e^{-(\kappa+\gamma)t}}{\kappa+\gamma}\sigma_\chi\sigma_\xi\rho_{\chi\xi} \\ \frac{1-e^{-(\kappa+\gamma)t}}{\kappa+\gamma}\sigma_\chi\sigma_\xi\rho_{\chi\xi} & \frac{1-e^{-2\gamma t}}{2\gamma}\sigma_\xi^2 \end{pmatrix}, \tag{2.6}$$

respectively. Hence, the logarithm of the spot price follows a normal distribution with its mean and variance of

$$\mathbb{E}[\ln(S_t)] = e^{-\kappa t}\chi_0 + \frac{\mu_\xi}{\gamma}\left(1 - e^{-\gamma t}\right) + e^{-\gamma t}\xi_0 + g(t), \tag{2.7}$$

and

$$Var[\ln(S_t)] = \frac{1-e^{-2\kappa t}}{2\kappa}\sigma_\chi^2 + 2\frac{1-e^{-(\kappa+\gamma)t}}{\kappa+\gamma}\sigma_\chi\sigma_\xi\rho_{\chi\xi} + \frac{1-e^{-2\gamma t}}{2\gamma}\sigma_\xi^2. \tag{2.8}$$

Since S_t follows a log-normal distribution, the logarithm of the expected value of the spot price at time t is

$$\ln(\mathbb{E}[S_t]) = \mathbb{E}[\ln(S_t)] + \frac{1}{2}Var[\ln(S_t)]. \tag{2.9}$$

2.1.2 Modelling the Spot Price under Risk-Neutral Measure

The key assumption in developing any pricing models for financial derivatives is that we estimate prices under the arbitrage-free market. That is, we assume that there are no riskless profits which can be made in any event of trades within this arbitrary market. As the probability distribution of an asset at maturity is known, one may think that the price of futures contract at time t may simply be the expectation of the spot price of an asset at maturity T under the same distribution. However, the known distribution takes into account the risk factors, which does not provide the true price of an asset in the arbitrage-free market. Hence, the risk-neutral probability measure is used, where the price will be adjusted so that it does not compensate for an investor's risk preference, Hull [29].

Under the risk-neutral probability measure, we incorporate two additional parameters, λ_χ and λ_ξ, where both parameters are price adjustments for χ_t and ξ_t, respectively. Under the risk-neutral probability measure, equations (2.2) and (2.3) now become

$$d\chi_t = (-\kappa\chi_t - \lambda_\chi)dt + \sigma_\chi dW_t^{\chi*}, \tag{2.10}$$

$$d\xi_t = (\mu_\xi - \lambda_\xi - \gamma\xi_t)dt + \sigma_\xi dW_t^{\xi*}, \tag{2.11}$$

where $W_t^{\chi*}$ and $W_t^{\xi*}$ are correlated standard Brownian processes, and $\mathbb{E}\left[dW_t^{\chi*}dW_t^{\xi*}\right] = \rho_{\chi\xi}dt$.

Performing similar derivation approach as in Section 2.1.1, the expectation and the variance of the joint distribution of χ_t and ξ_t are

$$\mathbb{E}^*[(\chi_t,\xi_t)] = \left(e^{-\kappa t}\chi_0 - \frac{\lambda_\chi}{\kappa}(1-e^{-\kappa t}), \frac{\mu_\xi-\lambda_\xi}{\gamma}\left(1-e^{-\gamma t}\right) + e^{-\gamma t}\xi_0\right), \tag{2.12}$$

$$Cov^*[(\chi_t,\xi_t)] = Cov[(\chi_t,\xi_t)] = \begin{pmatrix} \frac{1-e^{-2\kappa t}}{2\kappa}\sigma_\chi^2 & \frac{1-e^{-(\kappa+\gamma)t}}{\kappa+\gamma}\sigma_\chi\sigma_\xi\rho_{\chi\xi} \\ \frac{1-e^{-(\kappa+\gamma)t}}{\kappa+\gamma}\sigma_\chi\sigma_\xi\rho_{\chi\xi} & \frac{1-e^{-2\gamma t}}{2\gamma}\sigma_\xi^2 \end{pmatrix}, \tag{2.13}$$

where $\mathbb{E}^*$ and Cov^* are evaluated under the risk-neutral probability measure. The derivation of (2.12) and (2.13) are shown in Appendix A.1.

The logarithm of the spot price follows a normal distribution with its mean and variance of

$$\mathbb{E}^*[\ln(S_t)] = e^{-\kappa t}\chi_0 - \frac{\lambda_\chi}{\kappa}(1 - e^{-\kappa t}) + \frac{\mu_\xi - \lambda_\xi}{\gamma}\left(1 - e^{-\gamma t}\right) + e^{-\gamma t}\xi_0 + g(t), \tag{2.14}$$

$$Var^*[\ln(S_t)] = \frac{1 - e^{-2\kappa t}}{2\kappa}\sigma_\chi^2 + 2\frac{1 - e^{-(\kappa+\gamma)t}}{\kappa + \gamma}\sigma_\chi\sigma_\xi\rho_{\chi\xi} + \frac{1 - e^{-2\gamma t}}{2\gamma}\sigma_\xi^2. \tag{2.15}$$

Hence, the logarithm of the expected value of the spot price under the risk-neutral measure at time t is

$$\ln\left(\mathbb{E}^*[S_t]\right) = \mathbb{E}^*[\ln(S_t)] + \frac{1}{2}Var^*[\ln(S_t)]. \tag{2.16}$$

2.1.3 Modelling the Futures Price

We define a probability space denoted by $(\Omega, \Im, \mathbb{P})$, and by $\{\Im_t\}_{t\geq 0}$, a σ-algebra generated by the price process $\{S_t\}_{t\geq 0}$, which represents information up to time t. We assume that interest rates are deterministic. Under the risk-neutral framework, futures prices are equivalent to the expected spot prices in the future. That is, if we define $F_{t,T}$ to be the futures price at time t which matures at time T, then

$$F_{t,T} = \mathbb{E}^*\left[S_T|\Im_t\right]. \tag{2.17}$$

Hence, using (2.16) and (2.17), the futures price at time t with maturity at T is given by

$$\ln F_{t,T} = \ln\left(\mathbb{E}^*\left[S_T|\Im_t\right]\right) = e^{-\kappa(T-t)}\chi_t + e^{-\gamma(T-t)}\xi_t + A(T-t) + g(T), \tag{2.18}$$

where we define $A(t)$ to be

$$\begin{aligned} A(t) = &-\frac{\lambda_\chi}{\kappa}(1 - e^{-\kappa t}) + \frac{\mu_\xi - \lambda_\xi}{\gamma}(1 - e^{-\gamma t}) \\ &+ \frac{1}{2}\left(\frac{1 - e^{-2\kappa t}}{2\kappa}\sigma_\chi^2 + 2\frac{1 - e^{-(\kappa+\gamma)t}}{\kappa + \gamma}\sigma_\chi\sigma_\xi\rho_{\chi\xi} + \frac{1 - e^{-2\gamma t}}{2\gamma}\sigma_\xi^2\right). \end{aligned} \tag{2.19}$$

The derivation of (2.18) and (2.19) are provided in Appendix A.1. Now, since χ_t and ξ_t are jointly normally distributed, using (2.5) and (2.6), the expectation and the variance of the

logarithm of futures price are

$$\begin{aligned}
\mathbb{E}^*\left[\ln F_{t,T}\right] &= e^{-\kappa(T-t)}\mathbb{E}^*\left(\chi_t\right) + e^{-\gamma(T-t)}\mathbb{E}^*\left(\xi_t\right) + A(T-t) + g(T) \\
&= e^{-\kappa T}\chi_0 + e^{-\gamma T}\xi_0 + e^{-\kappa(T-t)}\left(1-e^{-\kappa t}\right)\frac{\lambda_\chi}{\kappa} \\
&+ e^{-\gamma(T-t)}\left(1-e^{-\gamma t}\right)\frac{\mu_\xi - \lambda_\xi}{\gamma} + A(T-t) + g(T), \\
Var^*\left[\ln F_{t,T}\right] &= e^{-2\kappa(T-t)}Var^*\left(\chi_t\right) + e^{-2\gamma(T-t)}Var^*\left(\xi_t\right) + 2e^{-(\kappa+\gamma)(T-t)}Cov^*\left[(\chi_t,\xi_t)\right] \\
&= e^{-2\kappa(T-t)}\sigma_\chi^2\frac{1-e^{-2\kappa t}}{2\kappa} + e^{-2\gamma(T-t)}\sigma_\xi^2\frac{1-e^{-2\gamma t}}{2\gamma} \\
&+ 2e^{-(\kappa+\gamma)(T-t)}\frac{1-e^{-(\kappa+\gamma)t}}{\kappa+\gamma}\sigma_\chi\sigma_\xi\rho_{\chi\xi}.
\end{aligned}$$

Note that we can deseasonalise the futures price by rearranging $g(T)$ to the left-hand side in (2.18), so that

$$\ln F_{t,T} - g(T) = \ln \tilde{F}_{t,T} = e^{-\kappa(T-t)}\chi_t + e^{-\gamma(T-t)}\xi_t + A(T-t). \tag{2.20}$$

Then, working on deseasonalised futures prices $\tilde{F}_{t,T}$, we can assume the seasonal function $g(t) = 0$ in (2.7), (2.14) and (2.18).

2.1.4 Parameter Estimation

For parameter estimation, we first set up the model as a linear state-space model. Two latent variables are expressed in the state equation, and the relationship between state variables and futures prices are expressed in the measurement equation. Then, we implement the Kalman filter to estimate values of latent variables, and the marginal likelihood function to estimate parameters.

The linear state-space form for the pricing model is

$$\mathbf{x}_t = \mathbf{c} + \mathbf{G}\mathbf{x}_{t-1} + \mathbf{w}_t, \tag{2.21}$$

$$\mathbf{y}_t = \mathbf{d}_t + \mathbf{F}_t'\mathbf{x}_t + \mathbf{v}_t, \tag{2.22}$$

where, for $t = 1, 2, ..., n$ and for N contracts with different maturities $T_1, \ldots, T_N$ with $T_1 < T_2 < \ldots < T_N$, and

$$\mathbf{x}_t = \begin{pmatrix} \chi_t \\ \xi_t \end{pmatrix},\ \mathbf{c} = \begin{pmatrix} 0 \\ \frac{\mu_\xi(1-e^{-\gamma\Delta t})}{\gamma} \end{pmatrix},\ \mathbf{G} = \begin{pmatrix} e^{-\kappa\Delta t} & 0 \\ 0 & e^{-\gamma\Delta t} \end{pmatrix}, \tag{2.23}$$

$$\mathbf{y}_t = \left(\ln F_{t,T_1}, \ln F_{t,T_2}, \cdots, \ln F_{t,T_N}\right)',$$
$$\mathbf{d}_t = \left(A(T_1 - t) + g(T_1), A(T_2 - t) + g(T_2), \cdots, A(T_N - t) + g(T_N)\right)',$$
$$\mathbf{F}_t = \begin{pmatrix} e^{-\kappa(T_1-t)} & \cdots & e^{-\kappa(T_N-t)} \\ e^{-\gamma(T_1-t)} & \cdots & e^{-\gamma(T_N-t)} \end{pmatrix},$$

where $A(t)$ is as defined in (2.19), and Δt is the time difference in years between $t-1$ and t. For error terms $\mathbf{w}_t$ and $\mathbf{v}_t$, we assume

$$\mathbf{w}_t \sim \mathcal{N}(0, \mathbf{W}),\ \mathbf{v}_t \sim \mathcal{N}(0, \mathbf{V}), \tag{2.24}$$

where

$$\mathbf{W} = \begin{pmatrix} \frac{1-e^{-2\kappa\Delta t}}{2\kappa}\sigma_\chi^2 & \frac{1-e^{-(\kappa+\gamma)\Delta t}}{\kappa+\gamma}\sigma_\chi\sigma_\xi\rho_{\chi\xi} \\ \frac{1-e^{-(\kappa+\gamma)\Delta t}}{\kappa+\gamma}\sigma_\chi\sigma_\xi\rho_{\chi\xi} & \frac{1-e^{-2\gamma\Delta t}}{2\gamma}\sigma_\xi^2 \end{pmatrix}, \tag{2.25}$$

$$\mathbf{V} = \begin{pmatrix} s_{11}^2 & s_{12} & \cdots & s_{1N} \\ s_{12} & s_{22}^2 & \cdots & s_{2N} \\ \vdots & \vdots & \ddots & \vdots \\ s_{1N} & s_{2N} & \cdots & s_{NN}^2 \end{pmatrix}. \tag{2.26}$$

We denote s_{jj}^2 as variances of measurement errors for contract j, and s_{jk} as covariances of measurement errors between contracts j and k, where $j \neq k$. Further, we assume that $\mathbf{w}_t$ and $\mathbf{v}_t$ are independent of each other.

The unknown parameter set $\psi = \left(\kappa, \sigma_\chi, \lambda_\chi, \gamma, \mu_\xi, \sigma_\xi, \lambda_\xi, \rho_{\chi\xi}, \mathbf{V}\right)$ is estimated by optimising the log-likelihood function of $\mathbf{y}$, the joint distribution of $(\mathbf{y}_1, \mathbf{y}_2, \ldots, \mathbf{y}_n)$, with respect to ψ. The log-likelihood function is

$$\ell(\psi; \mathbf{y}) = \sum_{t=1}^{n} p(\mathbf{y}_t | \Im_{t-1}), \tag{2.27}$$

where $p(\mathbf{y}_t|\Im_{t-1})$ is the logarithm of the conditional probability density of $\mathbf{y}_t$ given information available until time $t-1$. Now, assuming that the prediction error $\mathbf{e}_t = \mathbf{y}_t - \mathbb{E}\left[\mathbf{y}_t|\Im_{t-1}\right]$ follows a multivariate normal distribution, the log-likelihood function in (2.27) can be re-expressed as

$$\ell(\psi; \mathbf{y}) = -\frac{Nn}{2}\ln(2\pi) - \frac{1}{2}\sum_{t=1}^{n}\left[\ln(\det(\mathbf{L}_{t|t-1})) + \mathbf{e}_t'\mathbf{L}_{t|t-1}^{-1}\mathbf{e}_t\right], \tag{2.28}$$

where $\mathbf{L}_{t|t-1} = Cov\left(\mathbf{e}_t|\Im_{t-1}\right)$, and $\det(\cdot)$ denotes the determinant of a matrix. Then, parameter estimates are obtained by maximising (2.28) with respect to ψ jointly.

Kalman Filter

To obtain the quantity for the log-likelihood function in (2.28), we need to estimate latent state vectors and their covariance matrices at each time t. We use the Kalman filter, a recursive procedure applied in the state-space model, for estimating state vectors which are functions of the measurement variable.

For the rest of the paper, we notate $\mathbf{B}_{t|s}$ to be a vector or a matrix $\mathbf{B}$ at time t, given information up to time s. To initialise the process, we first need to define the initial distribution for the state vector. A prior mean $\mathbb{E}\left(\mathbf{x}_{1|0}\right) = \mathbf{a}_{1|0}$, and covariance matrix $Var\left(\mathbf{x}_{1|0}\right) = \mathbf{P}_{1|0}$ need to be defined based on the observed mean and covariance in the data. Also, depending on the assumed behaviour of each latent variable, an appropriate initial value of the state vector can be selected. Under the extended Schwartz-Smith two-factor model, Binkowski et al. [8] suggests an appropriate initial distribution of the state vector, where the expectation and the covariance matrix are

$$\mathbb{E}(\mathbf{x}_{1|0}) = \mathbf{a}_{1|0} = \begin{pmatrix} 0 \\ \frac{\mu_\xi}{\gamma} \end{pmatrix}, \tag{2.29}$$

$$Cov(\mathbf{x}_{1|0}) = \mathbf{P}_{1|0} = \begin{pmatrix} \frac{\sigma_\chi^2}{2\kappa} & \frac{\sigma_\chi \sigma_\xi \rho_{\chi\xi}}{\kappa+\gamma} \\ \frac{\sigma_\chi \sigma_\xi \rho_{\chi\xi}}{\kappa+\gamma} & \frac{\sigma_\xi^2}{2\gamma} \end{pmatrix}, \tag{2.30}$$

respectively. In addition, Binkowski et al. [7] has detected the parameter identification problem within the log-likelihood function in the Kalman filter, which requires a modification in the optimisation procedure by introducing an additional constraint in the parameter estimation step. The constraint $\kappa \geq \gamma$ is considered, as the rate of mean-reversion of the short-term price deviation χ_t dominates the rate of mean-reversion of the long-term equilibrium price ξ_t.

The detailed steps for the Kalman filter are as follows.

1. Define the initial distribution of the state variables, $\mathbf{a}_{1|0}$ and $\mathbf{P}_{1|0}$.

2. Use $\mathbf{y}_t$ to compute the prediction error

$$\mathbf{e}_t = \mathbf{y}_t - \mathbb{E}\left[\mathbf{y}_t | \Im_{t-1}\right] = \mathbf{y}_t - \mathbf{d}_t - \mathbf{F}_t' \mathbf{a}_{t|t-1}, \tag{2.31}$$

   and the covariance matrix of the prediction error,

$$\mathbf{L}_{t|t-1} = \mathbf{F}_t' \mathbf{P}_{t|t-1} \mathbf{F}_t + \mathbf{V}. \tag{2.32}$$

Algorithm 1: Kalman filter and estimation of parameters

Input: $\psi_0, s_0, \mathbf{a}_{1|0}, \mathbf{P}_{1|0}, \Delta t, n, N$

Output: $\hat{\psi} = \left(\hat{\kappa}, \hat{\sigma}_\chi, \hat{\lambda}_\chi, \hat{\gamma}, \hat{\mu}, \hat{\sigma}_\xi, \hat{\lambda}_\xi, \hat{\rho}_{\chi\xi}, \hat{\mathbf{V}}\right)$

for $t \leftarrow 1$ ***to*** n **do**

  Prediction: Compute $\mathbf{e}_t, \mathbf{L}_{t|t-1}$ and $\det(\mathbf{L}_{t|t-1})$

  Filtering: Update $\mathbf{a}_t, \mathbf{P}_t$

  Compute ℓ_t

Maximise $\ell(\psi; \mathbf{y})$

return $\hat{\psi}$

3. Update the distribution of state variables.

$$\mathbf{a}_t = \mathbf{a}_{t|t-1} + \mathbf{K}_t \mathbf{e}_t, \tag{2.33}$$

$$\mathbf{P}_t = (\mathbf{I} - \mathbf{K}_t \mathbf{F}_t') \mathbf{P}_{t|t-1}, \tag{2.34}$$

where $\mathbf{I}$ is the identity matrix, and $\mathbf{K}_t$ is the Kalman gain, mathematically defined as

$$\mathbf{K}_t = \mathbf{P}_{t|t-1} \mathbf{F}_t (\mathbf{L}_{t|t-1})^{-1} \tag{2.35}$$

4. Compute the log-likelihood function at time t, where

$$\ell_t = -\ln\left(\det(\mathbf{L}_{t|t-1})\right) - \mathbf{e}_t' \mathbf{L}_{t|t-1}^{-1} \mathbf{e}_t. \tag{2.36}$$

5. Forecast distributions of the state vector for use in the subsequent filtering process. The expected value and the covariance matrix of the updated state vector are

$$\mathbf{a}_{t+1|t} = \mathbf{c} + \mathbf{G}\mathbf{a}_t, \tag{2.37}$$

$$\mathbf{P}_{t+1|t} = \mathbf{P}_{t|t-1} - \mathbf{G}\mathbf{P}_t\mathbf{G}' + \mathbf{W}. \tag{2.38}$$

6. Repeat steps 2-5 at each time point t for $t = 1, \ldots, n$. Then, the log-likelihood $\ell(\psi; \mathbf{y})$ is the sum of all log-likelihood functions calculated in step 4. i.e. $\sum_{t=1}^{n} \ell_t = \ell(\psi; \mathbf{y})$.

Once we obtain the log-likelihood function, we maximise it to obtain relevant parameter estimates. Depending on the model assumption, elements in $\mathbf{c}, \mathbf{G}, \mathbf{W}, \mathbf{d}_t, \mathbf{F}_t$ and $\mathbf{V}$ will differ.

Kalman Smoother

Kalman smoother is another method used to estimate values of latent state variables based on the filtered values as the result of using the Kalman filter. It is a backward smoothing method which was developed by Rauch et al. [36]. The detailed steps for Kalman smoother using this method are as follows.

1. Starting from the filtered values of latent variables $\mathbf{a}_{t|n}$ and $\mathbf{P}_{t|n}$ at time $t = n$, compute the estimate of latent variables for time $t-1$. Define $\mathbf{J}_t$ to be a matrix at time t, where

$$\mathbf{J}_{t-1} = \mathbf{P}_{t-1|t-1}\mathbf{G}'\mathbf{P}_{t|t-1}^{-1}. \tag{2.39}$$

   Then, the estimate of latent variables using the Kalman smoother is computed by

$$\mathbf{a}_{t-1|n} = \mathbf{a}_{t-1|t-1} + \mathbf{J}_{t-1}\left(\mathbf{a}_{t|n} - \mathbf{a}_{t|t-1}\right). \tag{2.40}$$

2. The covariance matrix of latent variables at time $t-1$ is computed by

$$\mathbf{P}_{t-1|n} = \mathbf{P}_{t-1|t-1} + \mathbf{J}_{t-1}\left(\mathbf{P}_{t|n} - \mathbf{P}_{t|t-1}\right)\mathbf{J}_{t-1}'. \tag{2.41}$$

3. Repeat steps 1-2 at each time point t for $t = n-1, \ldots, 1$.

However, a problem arises when we deal with a higher dimension of state variables, as this smoother requires the computation of an inverse matrix $\mathbf{P}_{t|t-1}^{-1}$. Hence, in the case when there are several state variables, the potential problem can be remedied using the Modified Bryson-Frazier smoother (MBF), [6]. The detailed steps for this approach are as follows.

1. The estimate of the state variables at time t is computed by

$$\mathbf{a}_{t|n} = \mathbf{a}_{t|t-1} + \mathbf{P}_{t|t-1}\mathbf{r}_{t-1}, \tag{2.42}$$

   where

$$\mathbf{r}_{t-1} = \mathbf{F}_t\mathbf{L}_{t|t-1}^{-1}\mathbf{e}_t + \left(\mathbf{G} - \mathbf{G}\mathbf{K}_t\mathbf{F}_t\right)'\mathbf{r}_t$$

   and $\mathbf{r}_n = 0$.

2. The covariance matrix of the latent variable at time t is computed by

$$\mathbf{P}_{t|n} = \mathbf{P}_{t|t-1} - \mathbf{P}_{t|t-1}\mathbf{R}_{t-1}\mathbf{P}_{t|t-1}, \tag{2.43}$$

   where

$$\mathbf{R}_{t-1} = \mathbf{F}_t\mathbf{L}_{t|t-1}^{-1}\mathbf{F}_t' + \left(\mathbf{G} - \mathbf{G}\mathbf{K}_t\mathbf{F}_t\right)'\mathbf{R}_t\left(\mathbf{G} - \mathbf{G}\mathbf{K}_t\mathbf{F}_t\right),$$

   and $\mathbf{R}_n = 0$.

3. Repeat steps 1-2 for all observations $t \in [1, n]$.

Once we obtain estimates of state variables, we can obtain estimated prices of futures contracts for different maturities. By comparing with actual futures prices, the performance of models using filtered and smoothed estimates of latent variables will be compared in Section 3.4.

2.1.5 Estimation of Covariance Matrix V

Recall, the covariance matrix of measurement errors $\mathbf{V}$ in (2.26) was

$$\mathbf{V} = \begin{pmatrix} s_{11}^2 & s_{12} & \cdots & s_{1N} \\ s_{12} & s_{22}^2 & \cdots & s_{2N} \\ \vdots & \vdots & \ddots & \vdots \\ s_{1N} & s_{2N} & \cdots & s_{NN}^2 \end{pmatrix}.$$

For estimation of covariances of measurement errors, instead of directly estimating each element in $\mathbf{V}$, we estimate correlation coefficients of measurement errors between different contracts, and convert them back to covariances. Let $\mathbf{V}$ and $\mathbf{R}$ represent covariance and correlation matrix of measurement errors, respectively, and let D be the diagonal matrix, where $\mathbf{D} = \text{diag}\left(s_{11}^2, \ldots, s_{NN}^2\right)$. The relationship between covariance and correlation matrix is

$$\mathbf{V} = \mathbf{D}^{\frac{1}{2}}\mathbf{R}\mathbf{D}^{\frac{1}{2}}. \tag{2.44}$$

We use the estimation approach introduced in Gürtler et al. [26] for correlation coefficients, which is often used in credit risk modelling. Let $\mathbf{z}_j$ be the normalised prices of the contract j, so that the vector of prices consists of $\mathbf{z} = (\mathbf{z}_1, \mathbf{z}_2, \ldots, \mathbf{z}_N)$ for N contracts. We assume that

$$\mathbf{z}_j = \rho_j \varepsilon_0 + \sqrt{1 - \rho_j^2}\varepsilon_j, \ j = 1, \ldots, N, \tag{2.45}$$

where $\varepsilon = (\varepsilon_0, \ldots, \varepsilon_N) \sim N(0, \mathbf{I}_{N+1})$, ε_0 is a systematic component and $\varepsilon_1, \ldots, \varepsilon_N$ are idiosyncratic components. Therefore,

$$Corr\left[(\mathbf{z}_j, \mathbf{z}_k)\right] = \rho_j \rho_k, \ (j, k) = 1, \ldots, N, \ j \neq k. \tag{2.46}$$

In this setup, we have the following correlation matrix structure

$$\mathbf{R} = \begin{pmatrix} 1 & \rho_1\rho_2 & \rho_1\rho_3 & \cdots & \rho_1\rho_N \\ \rho_1\rho_2 & 1 & \rho_2\rho_3 & \cdots & \rho_2\rho_N \\ \rho_1\rho_3 & \rho_2\rho_3 & 1 & \cdots & \rho_3\rho_N \\ \vdots & \vdots & \vdots & \ddots & \vdots \\ \rho_1\rho_N & \rho_2\rho_N & \cdots & \rho_{N-1}\rho_N & 1 \end{pmatrix}. \tag{2.47}$$

Hence, in the parameter estimation, the modified covariance matrix $\mathbf{V}$ is applied in the Kalman filter procedure, and estimating both volatilities of different futures contracts, as well as correlation coefficients defined in (2.47) are required.

2.1.6 Volatility Parametrisation

For calibration of price data with N contracts, volatilities of measurement errors for each contract, $s_{11}, \ldots, s_{NN}$ need to be estimated. As we increase the number of contracts, the dimensionality in the parameter set also increases. With further increase in the number of parameters due to correlation coefficients introduced in Section , the estimation process leads to a computational challenge with a lack of efficiency.

To resolve this issue, we introduce a parametric function for volatilities of measurement errors. Let $s(j)$ be the volatility of the measurement error for $j = 1, \ldots, N$, and T_j be the maturity for j-th contract in years. Then, volatilities of measurement errors are expressed as an exponential function in terms of maturity, such that

$$s(j) = v_1 + v_2 e^{v_3 T_j}, \quad \text{where } v_1, v_2 > 0, v_3 \in \mathbb{R}, s_{jj} = s(j). \tag{2.48}$$

The advantage of using maturity-dependent volatility for measurement errors is that it reduces the dimensionality by $N - 3$. In a large set of price data, with a large number of N contracts with different maturities being traded, this estimation method increases the time efficiency in estimation step, and simple calculations can be done for volatilities of measurement errors based on estimates of v_1, v_2 and v_3.

2.2 Overview of Models 1 and 2

For the purpose of comparing different models, we describe existing reduced-form models based on the extended Schwartz-Smith two-factor model.

2.2.1 Model 1 - One-Factor GBM

The stochastic differential equation of the geometric Brownian motion, in terms of the price process $\{S_t\}_{t\geq 0}$ is

$$dS_t = \mu S_t dt + \sigma S_t dW_t.$$

Under the risk-neutral probability measure, the above process is expressed as

$$dS_t = (\mu - \lambda) S_t dt + \sigma S_t dW_t^*, \tag{2.49}$$

and the solution to (2.49) is simply

$$\ln S_t = \ln S_0 + (\mu - \lambda - \frac{1}{2}\sigma^2)t + \sigma W_t^*. \tag{2.50}$$

The single-factor GBM model can similarly be thought of as the Schwartz-Smith two-factor model, where $\chi_t = 0$. That is, the logarithm of the spot price is simply given as

$$\ln S_t = \xi_t. \tag{2.51}$$

Now, (2.50) in terms of ξ_t is

$$\xi_t = \xi_0 + (\mu_\xi - \lambda_\xi - \frac{1}{2}\sigma_\xi^2)t + \sigma_\xi W_t^*, \tag{2.52}$$

and the expectation and the variance of ξ_t under the risk-neutral measure is

$$\mathbb{E}^*[\xi_t] = \xi_0 + (\mu_\xi - \lambda_\xi - \frac{1}{2}\sigma_\xi^2)t, \tag{2.53}$$

$$Var^*[\xi_t] = \sigma_\xi^2 t. \tag{2.54}$$

Hence, the logarithm of the futures price at time t which matures in time T is

$$\begin{aligned} \ln F_{t,T} &= \ln(\mathbb{E}^*[S_T]) = \mathbb{E}^*[\xi_T] + \frac{1}{2}Var^*[\xi_T] \\ &= \xi_0 + (\mu_\xi - \lambda_\xi - \frac{1}{2}\sigma_\xi^2)(T-t) + \frac{1}{2}\sigma_\xi^2(T-t) \\ &= \xi_0 + (\mu_\xi - \lambda_\xi)(T-t). \end{aligned} \tag{2.55}$$

By letting $\chi_t, \kappa, \sigma_\chi, \lambda_\chi, \rho_{\chi\xi}$ to be zero in the Kalman filter procedure, the same setup as the procedure for the Schwartz-Smith two-factor model is implemented. Only $\mathbf{c}$ and $A(t)$ from (2.23) and (2.19) need to be modified, where

$$\mathbf{c} = \begin{pmatrix} 0 \\ (\mu_\xi - \frac{1}{2}\sigma_\xi^2)\Delta t \end{pmatrix} \text{ and } A(t) = (\mu_\xi - \lambda_\xi)t.$$

2.2.2 Model 2 - The Schwartz-Smith Two Factor Model

The original work by Schwartz and Smith [37] is a special case of the model described in Section 2.1, with $\gamma = 0$. Consequently, ξ_t follows a Brownian motion. Under the risk-neutral probability measure, the stochastic differential equation for ξ_t is

$$d\xi_t = (\mu_\xi - \lambda_\xi)dt + \sigma_\xi dW_t^{\xi*}, \tag{2.56}$$

and no changes made to χ_t. With terms involving γ in the denominator in previous sections, Taylor expansion in the numerator needs to be considered. For example,

$$\begin{aligned}\lim_{\gamma\to 0}\frac{1-e^{-\gamma\Delta t}}{\gamma} &= \lim_{\gamma\to 0}\frac{1-(1-\gamma\Delta t+\gamma^2\Delta t^2-\ldots)}{\gamma}\\ &= \lim_{\gamma\to 0}\frac{\gamma\Delta t-\gamma^2\Delta t^2+\ldots}{\gamma} = \Delta t.\end{aligned}$$

In addition, measurement errors between different contracts are assumed to be independent of each other. That is, the covariance matrix $\mathbf{V}$ is simply diag $\left(s_{11}^2,\ldots,s_{NN}^2\right)$.

3

Application to EUA Futures Data

In this chapter, we calibrate the European Union Allowance (EUA) futures data using models described in Chapter 2, and conduct comparative analysis of the performance of different models.

3.1 Data Description

We consider the historical daily prices of EUA futures contracts traded in the Intercontinental Exchange from January 4, 2016 to August 31, 2020, obtained from Refinitiv Datascope. This period covers the second half of Phase III of the EU-ETS. We consider the first 10 available contracts from January 4, 2016 to April 29, 2020 for model calibration. The 12th, 13th and 14th contracts will be used for examining out-of-sample performance for longer-maturity contracts, and daily prices from April 30, 2020 to August 31, 2020 will be used for examining out-of-sample prediction for three months ahead.

The maturity pattern changes for available contracts at different time points. The first

three available contracts mature in 1, 2 and 3 months, respectively, and for the remaining contracts, they mature either in the next quarterly months (March, June, September and December) which comes after at least 3 months, or only in December for longer-maturity contracts. For example, for a futures contract traded on May 1, 2016, the first three contracts mature at the end of May, June and July 2016, and for consecutive contracts, they mature at the end of September 2016, December 2016, March 2017, and continues on. For the 12th, 13th and 14th available contracts, within the time period for model calibration, these are quarterly contracts due in 30, 33 and 36 months, respectively. However, as no quarterly contracts are being traded with expiries after March 2021, three contracts become December annual contracts when the next available contracts mature after this expiry date. For example, on October 1, 2018, 13th available contract matures on December 20, 2021, and 14th available contract matures on December 19, 2022.

Figure 3.1 shows the term structure of EUA futures prices, but we assign numbers to each subsequent contract, instead of maturities, due to changes in the maturity structure explained above. The number j is given to j-th available contract.

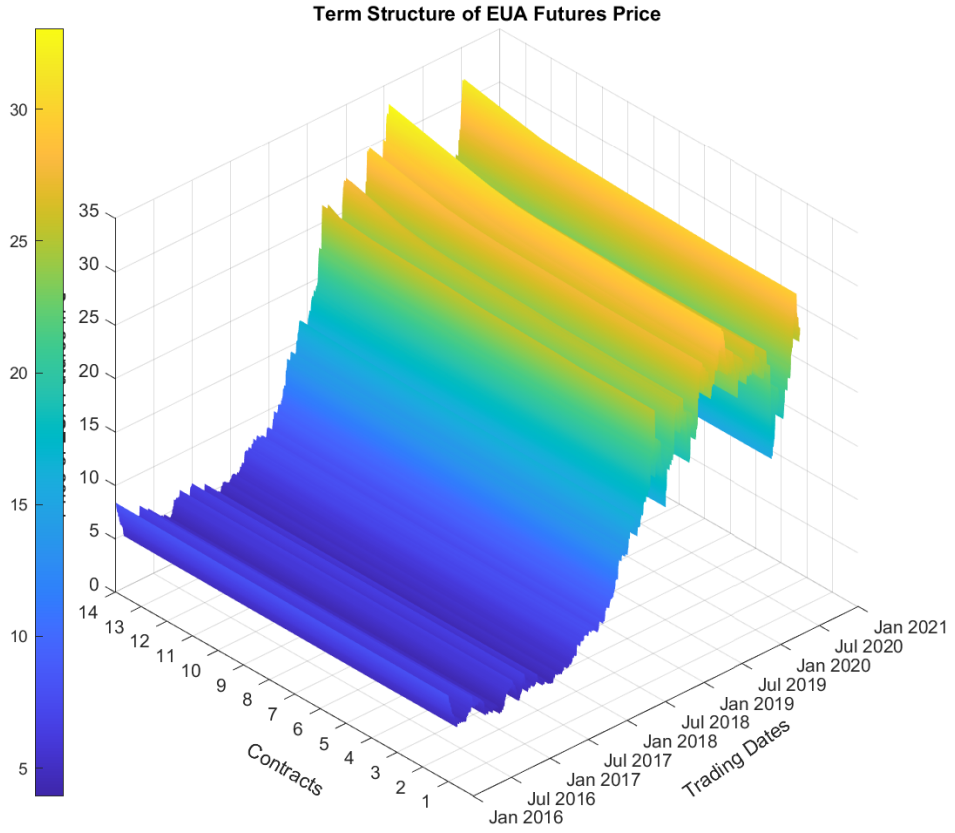

Figure 3.1: Term structure of EUA futures prices for 14 available contracts from January 4, 2016 to August 31, 2020

3.2 Deseasonalisation of Data

In this section, we briefly explain steps taken for deseasonalising the historical daily EUA futures prices.

3.2.1 Data Detrending

At first, we transform price into a log-scale. To linearly detrend the data, we fit the multivariate regression on the price data to obtain a single fitted line for all available contracts, with time t being the explanatory variable. This assumes that all contracts have the same slope δ, with the same intercept α. Define N to be the number of contracts, and n be the number of observations. Let $Y_{n\times N}$ be the logarithm of futures prices, and let the input X be an n-element cell array of $N \times K$ design matrices, where K is the number of regression coefficients which are to be estimated. In our case, $K = 2$ for one common intercept α, and one common slope δ. The t-th element in the cell X is

$$X_t = \begin{pmatrix} 1 & t \\ 1 & t \\ 1 & t \\ \vdots & \vdots \\ 1 & t \end{pmatrix}_{N\times 2} . \tag{3.1}$$

We use covariance-weighted least squares estimation, which allows covariance matrix of errors to be different from identity matrix. The result is equivalent to a simple linear regression with the data aggregated for all responses and predictor variables. Using the ordinary least squares method, we obtain the estimated coefficients and R^2 in Table 3.1.

Table 3.1: Regression coefficients

$\hat{\alpha}$	$\hat{\delta}$
1.3015	0.0020
(0.00513)	(8.025E-6)
$R^2 = 0.846$	

The plot of the price data with a fitted line is provided in Figure 3.2. It can clearly be seen that for all contracts, the regression line is fitted using one common slope δ. R^2 is almost

at 0.85, indicating that approximately 85% of the variability in the price for each available contract can be explained by time t, using this regression model. Hence, we linearly detrend the price data by subtracting the fitted linear function. At time t, the detrended price, defined as $\check{Y}_t$, is

$$\check{Y}_t = Y_t - \hat{\alpha} - \hat{\delta}t, \tag{3.2}$$

and the path of detrended price is shown in Figure 3.3.

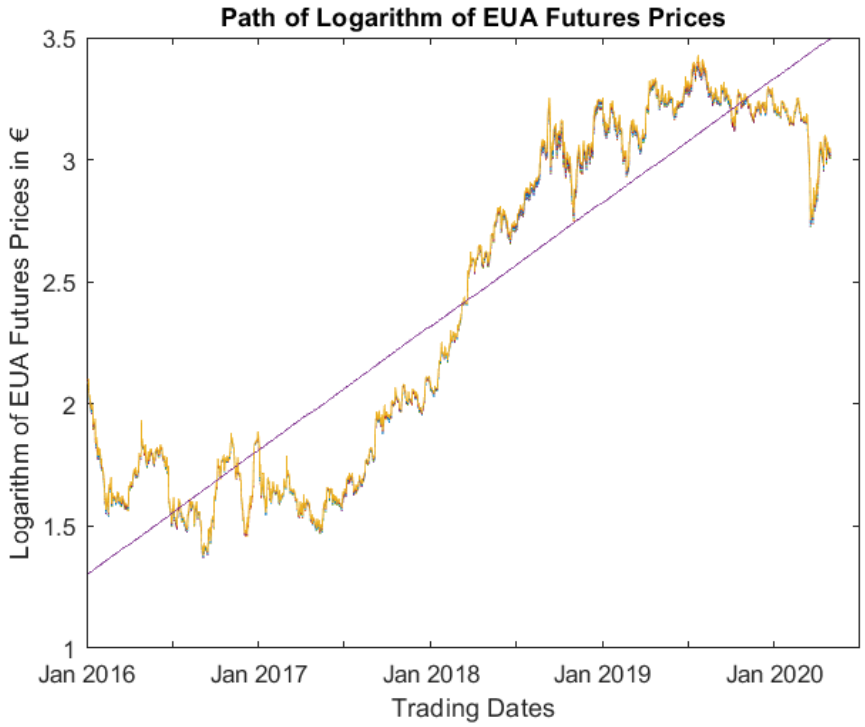

Figure 3.2: Path of logarithm of futures prices with a fitted line, for first 10 available contracts, from January 4, 2016 to April 29, 2020

3.2.2 Frequency Analysis

In this section, we perform a frequency-domain analysis. Recall, the sum of sinusoidal functions in $g(t)$ was expressed in (2.4) as

$$g(t) = \sum_{h=1}^{q} \left[a_h \cos\left(\frac{2\pi t}{A_h}\right) + b_h \sin\left(\frac{2\pi t}{A_h}\right) \right], \tag{3.3}$$

where, for q harmonics, A_h are periodicity for $h = 1, ..., q$.

To determine the frequency of cyclical pattern, we perform the spectral analysis on the detrended price. We convert a signal from the time domain to the frequency domain, and

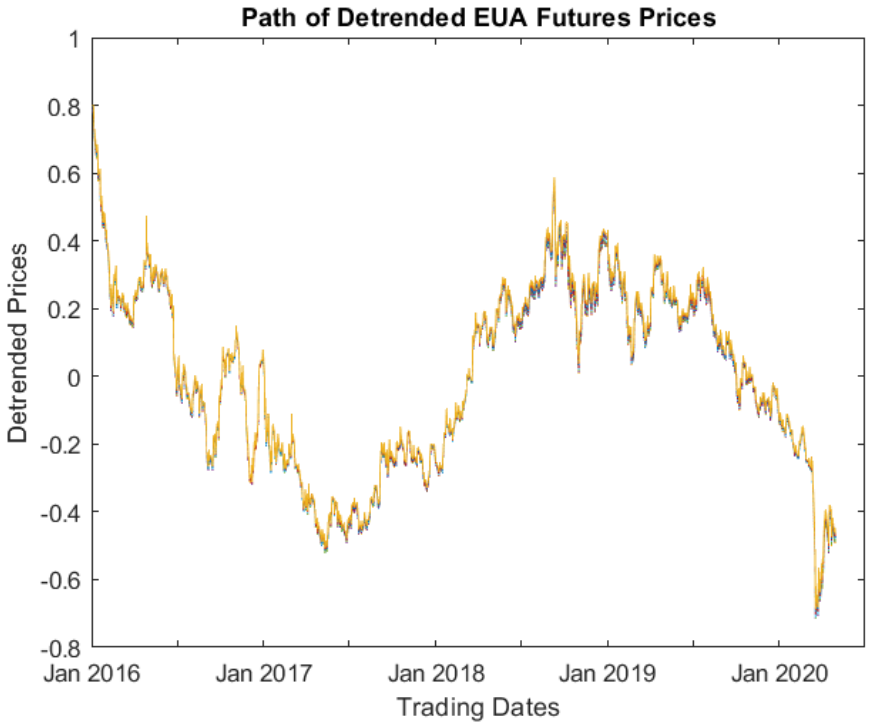

Figure 3.3: Path of detrended logarithm of futures prices for first 10 available contracts, from January 4, 2016 to April 29, 2020

implement Welch's method, Welch [45], for estimating the power spectral density. For illustration, the periodogram using the first available contract is shown in Figure 3.4. The plot suggests signals at frequencies of 47, 109, 150 and 185, and results were same for all 10 contracts considered for calibration. For interpretational purpose, we use 109 (approximately 3 months), 150 (approximately 5 months) and 185 (approximately 6 months). Each harmonic uses different frequencies, as in Green et al. [24]; for example, the first harmonic will have the periodicity of 3 months, the second harmonic has a five-month period, and the last harmonic has a six-month period. The multivariate non-linear fit on the detrended data is applied to obtain common estimates of coefficients applicable to all available contracts. We add the harmonics one at a time to fit the sum of sinusoid function to determine possible seasonality, and compare the adjusted R^2. Table 3.2 shows that the average of adjusted R^2 of all contracts increases as we add more harmonics up to three, but the goodness-of-fit does not improve afterwards.

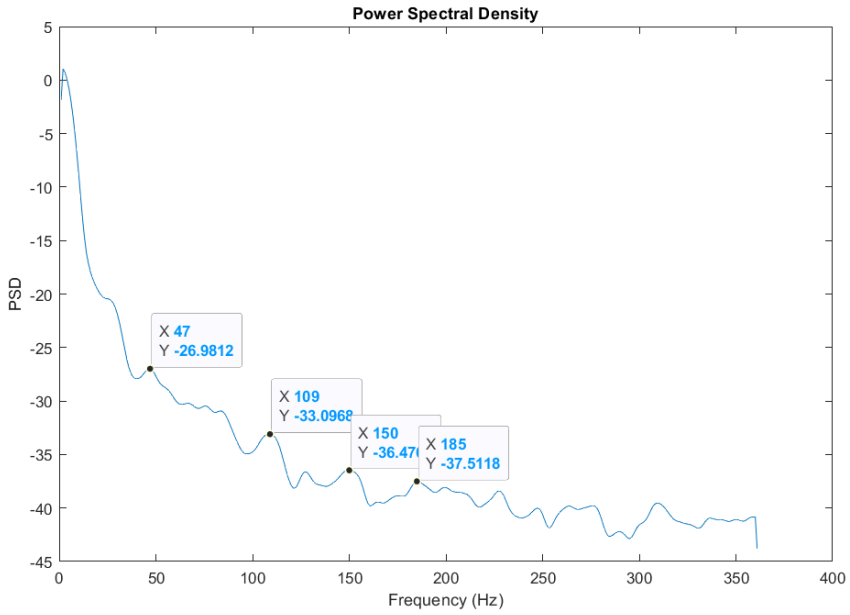

Figure 3.4: Power spectral density using detrended futures prices of first available contract

Table 3.2: Average of adjusted R^2 using different harmonics for different contracts

k	1	2	3	4
Periodicity	3 months	+ 6 months	+ 5 months	+2 months
Adj R^2	0.0045	0.0352	0.0410	0.0405

Hence, the estimated seasonal component $\hat{g}(t)$ is

$$\hat{g}(t) = \hat{a}_1 \cos\frac{2\pi t}{109} + \hat{b}_1 \sin\frac{2\pi t}{109} + \hat{a}_2 \cos\frac{2\pi t}{185} + \hat{b}_2 \sin\frac{2\pi t}{185} + \hat{a}_3 \cos\frac{2\pi t}{150} + \hat{b}_3 \sin\frac{2\pi t}{150} \quad (3.4)$$

and coefficients for each harmonic are given in Table 3.3.

Table 3.3: Non-linear regression coefficients

$\hat{a}_1$	$\hat{b}_1$	$\hat{a}_2$	$\hat{b}_2$	$\hat{a}_3$	$\hat{b}_3$
0.0070	0.0274	-0.0272	0.0672	0.0236	-0.0247

Subtracting $\hat{g}(t)$ from $\check{Y}_t$, we obtain the deseasonalised price, defined as $\tilde{Y}_t$, where

$$\tilde{Y}_t = \check{Y}_t - \hat{g}(t), \quad (3.5)$$

and this is used in the Kalman filter procedure for estimation of parameters. The plot of deseasonalised prices for the first available contract, along with seasonal component, is shown in Figure 3.5.

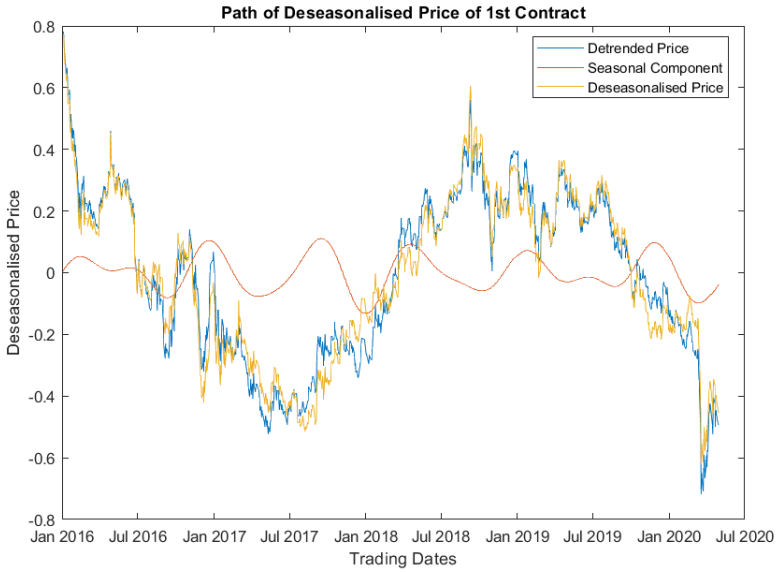

Figure 3.5: Deseasonalised prices of first available contract, along with seasonal component, from January 4, 2016 to April 29, 2020

3.3 Parameter Estimation

In this section, we present estimates of parameters for Models 1 to 5. To determine best initial values for parameter optimisation, we use the grid search. We first set the range for each parameter arbitrarily, and we set number of grid points for each parameter set. The lower and upper limits for each parameter are given in Table 3.4, and the initial values for each model are summarised in Table 3.5.

Table 3.4: Lower and upper bounds for each parameter in the model

	κ	σ_χ	λ_χ	γ	μ_ξ	σ_ξ	λ_ξ	$\rho_{\chi\xi}$
Lower limit	0	0	-5	0	-5	0	-5	-1
Upper limit	5	5	5	5	5	5	5	1

In addition, we let the set of volatilities $s_{jj} \in [0,1]$, $(v_1, v_2) \in [0,1]$, and $v_3 \in [-5,5]$, and the set of correlations $\rho_{jk} \in [-1,1]$, for contracts j and k, $j \neq k$.

Table 3.5: Initial values for each model

	κ	σ_χ	λ_χ	γ	μ_ξ	σ_ξ	λ_ξ	$\rho_{\chi\xi}$	s_j	ρ_{jk}	v_1, v_2	v_3
Model 1	·	·	·	·	0	1.25	2.5	·	0.01	·	·	·
Model 2	1.25	3.75	-2.5	0	2.5	3.75	2.5	-0.5	0.01	·	·	·
Model 3	3.75	1.25	-2.5	1.25	-2.5	3.75	-2.5	-0.5	0.01	·	·	·
Model 4	2.25	2.25	0.25	0.75	-2	2.25	0.75	0.5	0.01	0.9	·	·
Model 5	1.25	1.25	2.5	3.75	2.5	1.25	2.5	-0.5	·	0.9	0.001	-5

Standard Errors of Parameter Estimates

Standard errors for parameter estimates have been computed using the bootstrapping approach. The method we used is summarised below. Using obtained parameter estimates, we resample m number of simulated data set, with equal sample size as the data considered for calibration, and the same time-to-maturity at each time point t. The steps are summarised below.

1. Use the optimal estimates $\hat{\psi} = \left(\hat{\kappa}, \hat{\sigma}_\chi, \hat{\lambda}_\chi, \hat{\gamma}, \hat{\mu}_\xi, \hat{\sigma}_\xi, \hat{\lambda}_\xi, \hat{\rho}_{\chi\xi}, \hat{\mathbf{V}}\right)$ to simulate values of state variables $\mathbf{x}_t$, and hence futures prices $\mathbf{y}_t$ for $t = 1, \cdots, n$, using the state and measurement equations in (2.21) and (2.22).

2. Optimise and record the optimal estimates of the simulated data set.

3. Repeat Steps 1-2 for m times. Using m sets of optimised parameter estimates, the standard error for each parameter is calculated as

$$s.e._p(\hat{\psi}) = \sqrt{\frac{Var_p(\hat{\psi})}{m}}, \tag{3.6}$$

for p-th parameter in the parameter set $\hat{\psi}$.

For each model, we take $m = 2,000$ for computing standard errors. Parameter estimates are shown in Table 3.6. Volatilities and correlations of measurement errors are shown in Table 3.7, and calculated volatilities based on $\hat{v}_1, \hat{v}_2, \hat{v}_3$ for Model 5 are presented in Table 3.8. We denote C_j to be the j-th available futures contract, and estimates which are not specified in the model are replaced with $(\cdot)$.

Table 3.6: Parameter estimates for Models 1-5

	Model 1 (Std. error)	Model 2 (Std. error)	Model 3 (Std. error)	Model 4 (Std. error)	Model 5 (Std. error)
$\hat{\kappa}$	.	0.0027 (0.0002)	0.0250 (0.0257)	0.0545 (0.0037)	0.0273 (0.0191)
$\hat{\sigma}_\chi$	.	4.5208 (0.0207)	0.5430 (0.0176)	0.6364 (0.0150)	0.7640 (0.0247)
$\hat{\lambda}_\chi$	.	2.6201 (0.0153)	0.6716 (0.0345)	0.1519 (0.0376)	-0.1105 (0.0486)
$\hat{\gamma}$	.	.	0.0054 (0.0008)	0.0264 (0.0006)	0.0102 (0.0029)
$\hat{\mu}$	-0.1856 (0.0095)	-0.3466 (0.0171)	-0.0932 (0.0157)	-0.0902 (0.0165)	0.0736 (0.0212)
$\hat{\sigma}_\xi$	0.5936 (0.0023)	4.3484 (0.0212)	0.7657 (0.0165)	1.2106 (0.0157)	1.2035 (0.0232)
$\hat{\lambda}_\xi$	-0.0176 (0.0105)	-2.7965 (0.0212)	-0.3147 (0.0234)	0.0051 (0.0321)	0.2062 (0.0420)
$\hat{\rho}_{\chi\xi}$	.	-0.9918 (0.0003)	-0.7458 (0.0105)	-0.9454 (0.0065)	-0.8314 (0.0105)
$\hat{\nu}_1$	.	.	.	.	0.0256 (0.0005)
$\hat{\nu}_2$	.	.	.	.	0.0027 (0.0015)
$\hat{\nu}_3$	.	.	.	.	-9.3410 (0.0868)
NLL	-4.5947E+4	-5.5340E+4	-5.5209E+4	-5.5791E+4	-5.5358E+4
AIC	-9.1867E+4	-1.1065E+5	-1.1038E+5	-1.1153E+5	-1.1067E+5
BIC	-9.1802E+4	-1.1056E+5	-1.1029E+5	-1.1139E+5	-1.1057E+5

Table 3.7: Estimates of volatilities and correlations of measurement errors for Models 1-5

	Model 1 $\times 10^{-2}$ (Std. error)	Model 2 $\times 10^{-2}$ (Std. error)	Model 3 $\times 10^{-2}$ (Std. error)	Model 4 (Std. error)	Model 5		Model 1	Model 2	Model 3	Model 4 (Std. error)	Model 5 (Std. error)
$\hat{s}_1$	0.0800 (5.36E-6)	0.0715 (1.13E-4)	0.0723 (0.0006)	0.0200 (0.0015)	.	$\hat{\rho}_1$	.	.	.	0.9994 (0.0115)	0.9999 (0.0146)
$\hat{s}_2$	0.0573 (5.07E-6)	0.0417 (3.67E-5)	0.0409 (0.0006)	0.0199 (0.0013)	.	$\hat{\rho}_2$	.	.	.	0.9999 (0.0110)	0.9998 (0.0131)
$\hat{s}_3$	0.0568 (4.15E-6)	0.0586 (7.52E-5)	0.0587 (0.0004)	0.0195 (0.0009)	.	$\hat{\rho}_3$	.	.	.	0.9996 (0.0116)	0.9998 (0.0129)
$\hat{s}_4$	0.1389 (1.96E-6)	0.0893 (1.73E-5)	0.0908 (0.0006)	0.0189 (0.0004)	.	$\hat{\rho}_4$	.	.	.	0.9996 (0.0162)	0.9996 (0.0143)
$\hat{s}_5$	0.2637 (2.49E-6)	0.1315 (2.15E-4)	0.1354 (0.0008)	0.0188 (0.0006)	.	$\hat{\rho}_5$	.	.	.	0.9985 (0.0104)	0.9988 (0.0137)
$\hat{s}_6$	0.3482 (2.72E-6)	0.1375 (7.47E-5)	0.1375 (0.0010)	0.0189 (0.0013)	.	$\hat{\rho}_6$	.	.	.	0.9975 (0.0082)	0.9985 (0.0119)
$\hat{s}_7$	0.4528 (4.90E-6)	0.1077 (2.16E-5)	0.1082 (0.0005)	0.0191 (0.0028)	.	$\hat{\rho}_7$	.	.	.	0.9983 (0.0078)	0.9989 (0.0090)
$\hat{s}_8$	0.6355 (8.83E-6)	0.1065 (2.11E-5)	0.1077 (0.0006)	0.0192 (0.0026)	.	$\hat{\rho}_8$	.	.	.	0.9985 (0.0060)	0.9989 (0.0075)
$\hat{s}_9$	0.7861 (1.03E-5)	0.0822 (1.92E-5)	0.0865 (0.0010)	0.0198 (0.0028)	.	$\hat{\rho}_9$	.	.	.	0.9995 (0.0069)	0.9997 (0.0069)
$\hat{s}_{10}$	0.9791 (1.27E-5)	0.2213 (1.20E-4)	0.2254 (0.0014)	0.0209 (0.0030)	.	$\hat{\rho}_{10}$	.	.	.	0.9967 (0.0065)	0.9970 (0.0084)

Table 3.8: Estimates of volatilities for Model 5

Contract	C_1	C_2	C_3	C_4	C_5
Maturity	1-mth	2-mth	3-mth	6-mth	9-mth
T_j in years	$\frac{1}{12}$	$\frac{1}{6}$	$\frac{1}{4}$	$\frac{1}{2}$	$\frac{3}{4}$
$s_j = v_1 + v_2 e^{v_3 T_j}$	0.0268	0.0262	0.0258	0.0256	0.0256
Contract	C_6	C_7	C_8	C_9	C_{10}
Maturity	12-mth	15-mth	18-mth	21-mth	24-mth
T_j in years	1	$\frac{5}{4}$	$\frac{3}{2}$	$\frac{7}{4}$	2
$s_j = v_1 + v_2 e^{v_3 T_j}$	0.0256	0.0256	0.0256	0.0256	0.0256

3.4 Comparative Analysis

To compare performances of different models, we analyse in-sample performance for models' ability of calibration, and out-of-sample performance for models' ability of predicting prices. We use the root mean square error (RMSE) criterion, where

$$RMSE_j = \sqrt{\frac{1}{n}\sum_{t=1}^{n}(y_{tj} - \hat{y}_{tj})^2}, \tag{3.7}$$

for jth contract. y_{tj} is the actual price, and $\hat{y}_{tj}$ is the estimated price at time t for j-th contract. The estimated vector of futures price at time t is the expectation of the measurement equation (2.22), and is calculated by

$$\hat{\mathbf{y}}_t = \hat{\mathbf{d}}_t + \hat{\mathbf{F}}_t' \hat{\mathbf{x}}_t, \tag{3.8}$$

where $\hat{\mathbf{x}}_t$ is the estimated vector of latent state variables obtained through the Kalman filter or the Kalman smoother, and $\hat{\mathbf{d}}_t$ and $\hat{\mathbf{F}}_t$ are calculated using parameter estimates in Tables 3.6, 3.7 and 3.8.

3.4.1 In-sample Performance

Using the whole period considered for model calibration, estimated prices using different models and actual prices are compared. Using RMSE criterion in (3.7), results for in-sample performances for Models 1-5 are summarised in Table 3.9. We present the result for 7th, 8th, 9th and 10th available contracts for illustration. We also compare two different estimates of state variables using the Kalman filter (KF) and the MBF smoother.

Table 3.9: In-sample RMSE for Models 1-5

Contract	$\hat{\mathbf{x}}_t$	Model 1	Model 2	Model 3	Model 4	Model 5
C_7	KF	0.0045	0.0010	0.0010	0.0169	0.0230
	MBF	0.0045	0.0010	0.0010	0.0169	0.0228
C_8	KF	0.0063	0.0010	0.0010	0.0170	0.0231
	MBF	0.0063	0.0010	0.0010	0.0170	0.0229
C_9	KF	0.0079	0.0007	0.0007	0.0177	0.0233
	MBF	0.0079	0.0007	0.0007	0.0176	0.0231
C_{10}	KF	0.0098	0.0022	0.0022	0.0188	0.0238
	MBF	0.0098	0.0021	0.0022	0.0187	0.0236

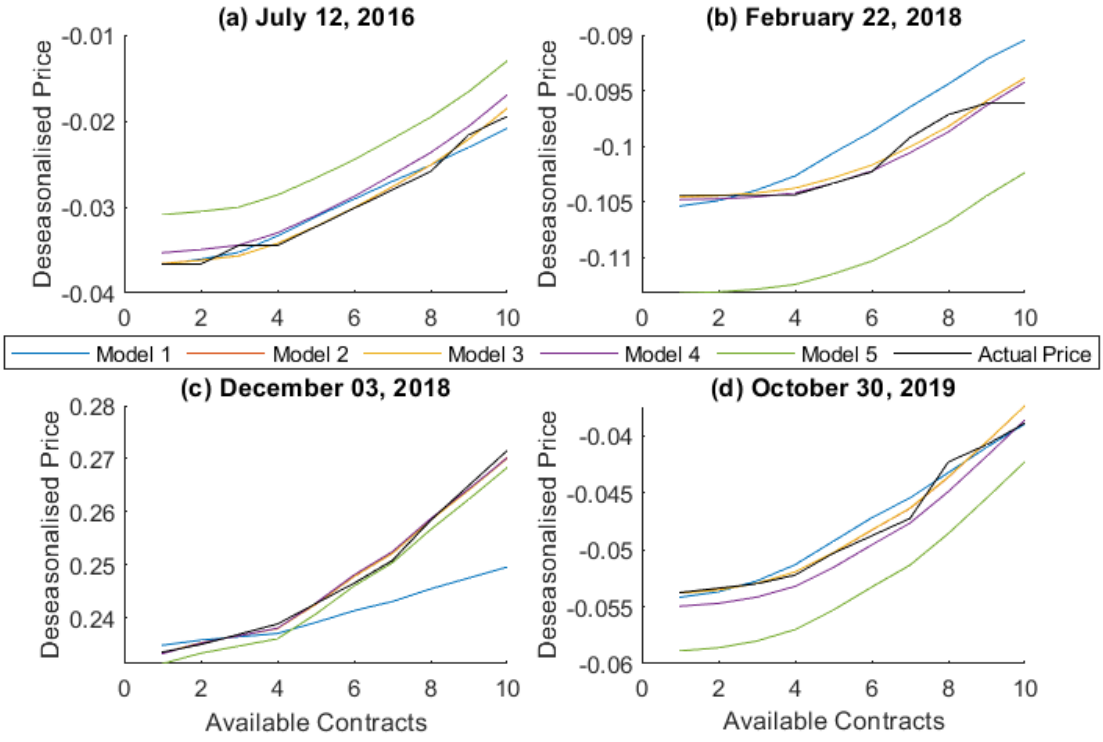

Figure 3.6: Fitted futures curves on (a) July 12, 2016, (b) February 22, 2018, (c) December 03, 2018, (d) October 30, 2019 for Models 1-5

The RMSE for tested contracts indicate that Models 1, 2, 3 fit the historical data very well, and Models 4 and 5 show slight deviations in fitted prices from actual futures price. All RMSE figures are quite low, showing that all models have ability to calibrate the historical data reasonably well. Slight differences can be seen between the use of filtered values and

smoothed values, but are negligible. The cross-sectional data of deseasonalised futures prices on four different trading dates are plotted in Figure 3.6. Presenting on the same scale as in Figure 3.1, the horizontal axis represents the j-th available contract, and the vertical axis represents both fitted and actual deseasonalised futures prices.

3.4.2 Out-of-sample Performance - Long-maturity Contracts

For this section, we use estimated parameters to predict prices for longer-maturity contracts. RMSEs for comparative analysis of out-of-sample performance are computed for Models 1-5, and results are given in Table 3.10.

Table 3.10: Out-of-sample RMSE for Models 1-5, for longer contracts

Contract	$\hat{\mathbf{x}}_t$	Model 1	Model 2	Model 3	Model 4	Model 5
C_{12}	KF	0.3275	0.0159	0.0039	0.0097	0.0501
	MBF	0.3275	0.0160	0.0047	0.0082	0.0485
C_{13}	KF	0.5039	0.0834	0.0559	0.0414	0.0033
	MBF	0.5039	0.0835	0.0568	0.0399	0.0047
C_{14}	KF	0.7195	0.2096	0.1547	0.0979	0.1019
	MBF	0.7195	0.2096	0.1558	0.0964	0.1033

A lack of predictability is shown when Model 1 is adapted, with much higher RMSE compared to Models 2-5. Models with two mean-reverting factors are preferrable, compared to Model 2. Better performances are shown in Models 4 and 5 which consider correlated measurement errors between contracts, with lower RMSE for Model 4. The prediction deviates quite significantly for each subsequent available contract, as the pattern of maturities change for the underlying EUAs in the period we are testing. For Model 4, using smoothed values for latent variables predicted better than filtered values, whereas for other models, filtered values performed better in most of contracts being considered. Futures curves on four different trading dates are shown in Figure 3.7.

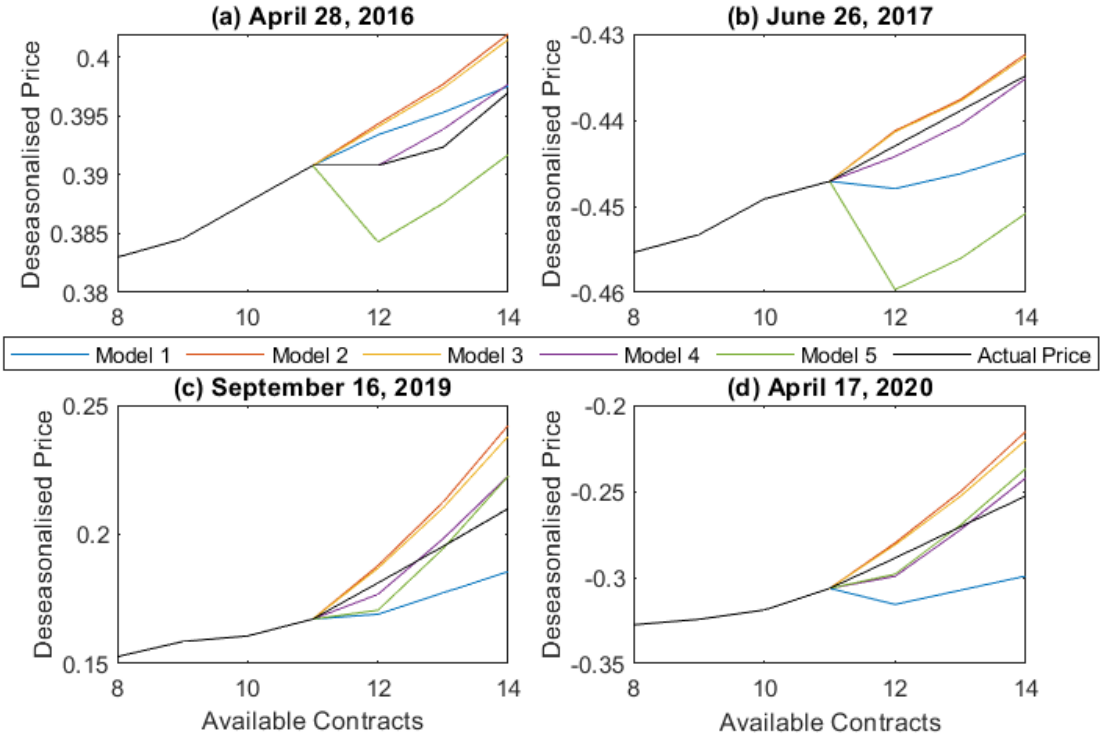

Figure 3.7: Fitted futures curves: Estimates of futures prices of longer-maturity contracts on (a) April 28, 2016, (b) June 26, 2017, (c) September 16, 2019 and (d) April 17, 2020, for Models 1-5

3.4.3 Out-of-sample Performance

Evaluating models in a different dimension, we now analyse the out-of-sample performance by predicting futures prices in the time domain. The steps for out-of-sample estimation are given below.

1. Based on the obtained estimates of parameters $\hat{\psi}$ and $\hat{\mathbf{x}}_t$, predict state variables using (2.37), for f-time-step ahead.
2. Using the measurement equation given in (3.8), estimate futures prices.

We use the historical daily prices of EUA futures contracts from 04/30/2020 to 08/31/20, and first 10 available contracts to assess the out-of-sample performance in the time domain. The same criterion in (3.7) is used, where $\hat{\mathbf{y}}_t$ is the vector of predicted futures prices at time t.

Table 3.11 summarises RMSEs for first 10 contracts. For the purpose of using a model to predict f-time-step ahead, Model 3 shows the lowest RMSE, followed by Model 4. Model

5 performs the worst, with its RMSE above 0.7. The main drawback of using Model 5 is that volatilities of measurement errors are highly over-estimated, compared to Models 1-3 in Table 3.7. Futures curves for four different trading dates are shown in Figure 3.8.

Table 3.11: Out-of-sample RMSE for Models 1-5, using predicted prices

Contract	Model 1	Model 2	Model 3	Model 4	Model 5
C_1	0.5489	0.5349	0.1356	0.3707	0.7660
C_2	0.5473	0.5303	0.1394	0.3664	0.7601
C_3	0.5456	0.5254	0.1434	0.3618	0.7540
C_4	0.5441	0.5178	0.1496	0.3546	0.7444
C_5	0.5458	0.5071	0.1578	0.3442	0.7300
C_6	0.5654	0.5097	0.1524	0.3469	0.7289
C_7	0.5778	0.5028	0.1566	0.3398	0.7184
C_8	0.5910	0.4955	0.1614	0.3322	0.7079
C_9	0.6127	0.4929	0.1608	0.3295	0.7022
C_{10}	0.6426	0.4947	0.1559	0.3311	0.7009

3.5 Diagnostic Checks

In this section, we perform diagnostic check of residuals for each model. Recall, in (2.24), measurement errors $\mathbf{v}_t$ are assumed to follow a multivariate normal distribution with mean 0 and variance matrix $\mathbf{V}$.

As $\mathbf{v}_t = (\mathbf{v}_{t1}, \mathbf{v}_{t2}, \ldots, \mathbf{v}_{tN})^T \sim \mathcal{N}_N$, a N-dimensional normal distribution for $t = 1, \ldots, n$, following the properties of multivariate normal distribution, the marginal distribution for each element in the vector $\mathbf{v}_t$ follows a univariate normal distribution. i.e. $\mathbf{v}_{tj} \sim \mathcal{N}_1$, for j-th contract, $j = 1, 2, \ldots, N$. Hence, their average will have to follow a normal distribution, since

$$\frac{1}{N}\sum_{j=1}^{N} \mathbf{v}_{tj} = \bar{\mathbf{v}}_t \sim \mathcal{N}_1.$$

Now, using $\bar{\mathbf{v}} = (\bar{\mathbf{v}}_1, \bar{\mathbf{v}}_2, \ldots, \bar{\mathbf{v}}_n)^T$, we check the normality assumption.

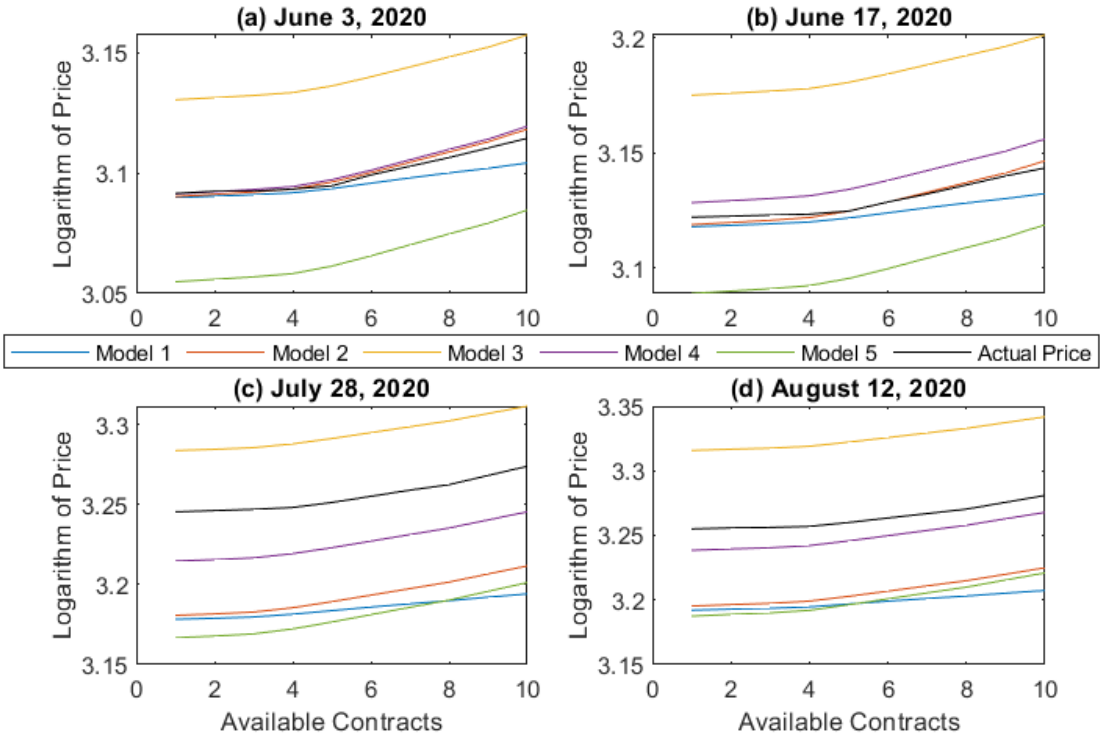

Figure 3.8: Fitted futures curves: 3-month estimates of futures prices on (a) June 3, 2020, (b) June 17, 2020, (c) July 28, 2020 and (d) August 12, 2020, for Models 1-5

Table 3.12: Summary statistics of average residuals for Models 1-5

Model #	Model 1	Model 2	Model 3	Model 4	Model 5
Mean	0.0006	-8.28E-6	-5.45E-6	-0.0004	0.0017
Median	-0.0002	-3.05E-5	-3.19E-5	4.33E-5	0.0049
StDev	0.0033	0.0002	0.0002	0.0173	0.0233
Max	0.0245	0.0013	0.0014	0.0453	0.0764
Min	-0.0038	-0.0008	-0.0008	-0.0931	-0.0878
Skewness	2.5872	0.4600	0.4683	-0.2781	-0.3222
Kurtosis	13.2370	4.3050	4.7054	3.7866	3.3423

Summary statistics for residuals from Models 1-5 are presented in Table 3.12. All residuals have their means very close to zero. Nonetheless, the summary statistics show Models 1-3 are moderately skewed, with excessive kurtosis. This property is also indicated by time series plots and quantile-quantile (Q-Q) plots with 95% confidence bands in Figures 3.9 to 3.13.

Model 1 clearly shows that residuals hugely deviate from normality, while Models 2, 3 and 5 seem reasonable, but shows cluster of residuals standing outside the 95% confidence band. Of all, Model 4 shows majority of residuals within the confidence band, with one observation, on October 29, 2018, which shows a large negative residual.

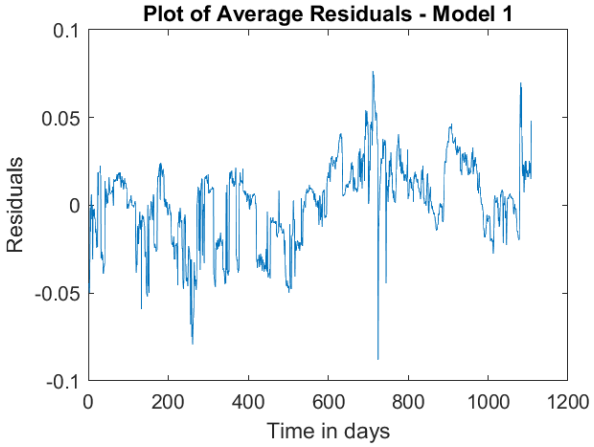

(a) Time series plot of residuals

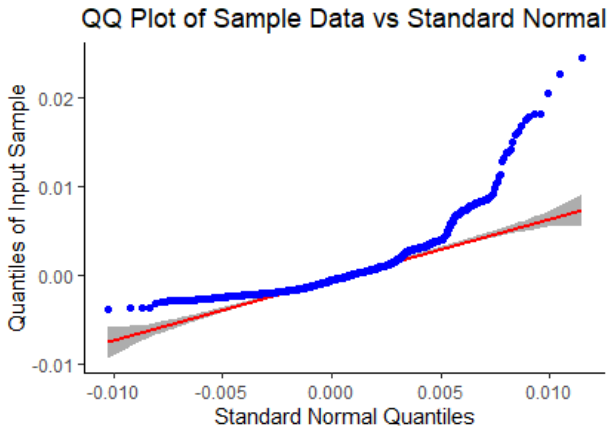

(b) Q-Q plot of residuals

Figure 3.9: Residual diagnostic plots for Model 1

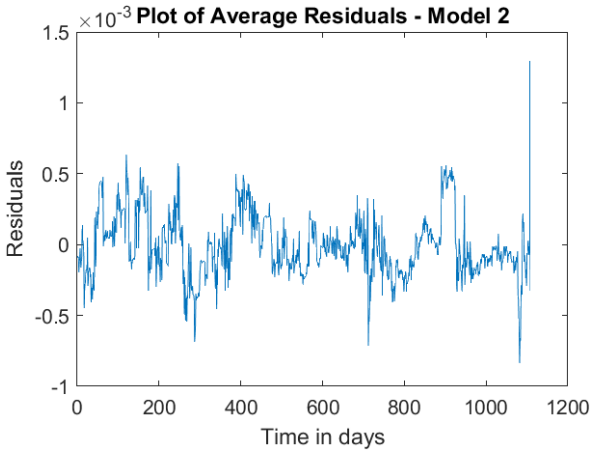

(a) Time series plot of residuals

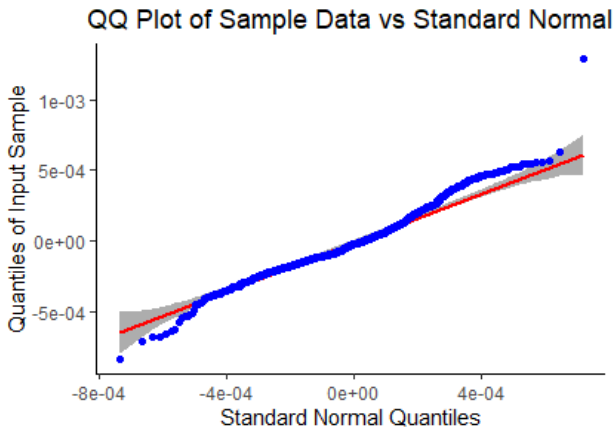

(b) Q-Q plot of residuals

Figure 3.10: Residual diagnostic plots for Model 2

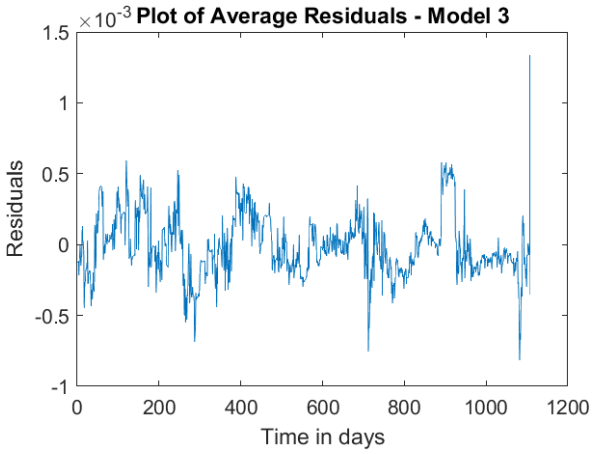

(a) Time series plot of residuals

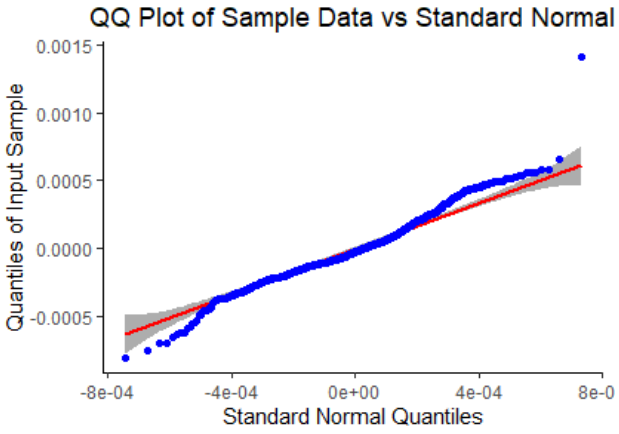

(b) Q-Q plot of residuals

Figure 3.11: Residual diagnostic plots for Model 3

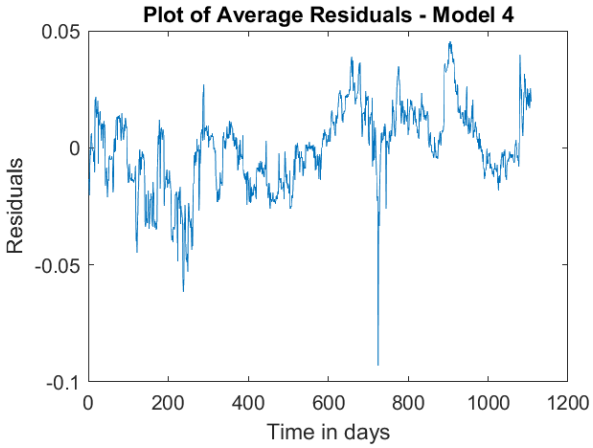

(a) Time series plot of residuals

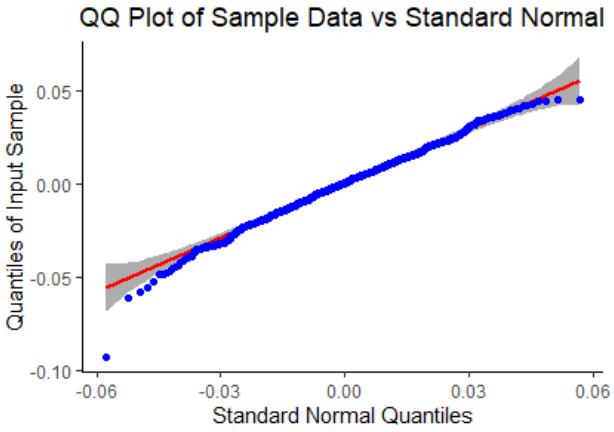

(b) Q-Q plot of residuals

Figure 3.12: Residual diagnostic plots for Model 4

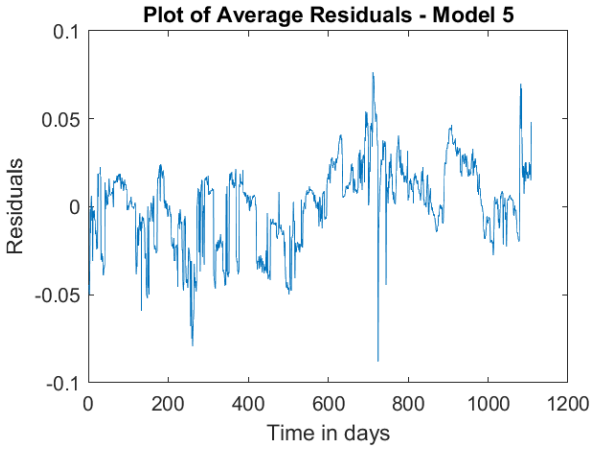

(a) Time series plot of residuals

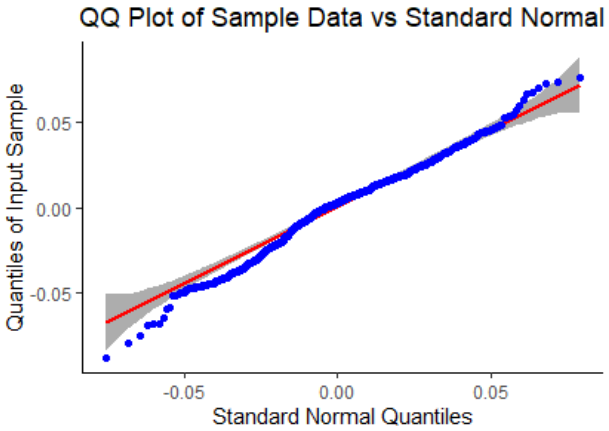

(b) Q-Q plot of residuals

Figure 3.13: Residual diagnostic plots for Model 5

We also perform a formal hypothesis test on normality assumption of residuals using the Anderson-Darling test. We remove any significant outliers shown in Figures 3.10, 3.11 and 3.12, which correspond to Models 2-4. The null hypothesis for this test is

$$H_0 : \text{Measurement errors are from a normal distribution} \tag{3.9}$$

Table 3.13: Summary of p-values of the Anderson-Darling test for Models 1-5

Model #	Model 1	Model 2	Model 3	Model 4	Model 5
p	< 0.0005	< 0.0005	< 0.0005	0.0605	< 0.0005

Computed p-values of the Anderson-Darling test to examine the normality assumption for residuals in Models 1-5 are given in Table 3.13. Model 4 shows that residuals may follow a normal distribution at 5% significance level, whereas for other models, it is clear that the normality assumption for residuals are not met. Hence, through diagnostic plots and a hypothesis test on normality, Model 4 satisfies the assumption on normality of measurement errors in (2.24).

4

Conclusion and Further Work

This thesis has reviewed five pricing models, based on the Schwartz-Smith two-factor model, Schwartz and Smith [37]. The first model, Model 1, assumes that the logarithm of the spot price follows a geometric Brownian motion. The second model, Model 2, assumes that the spot price is composed of a mean-reverting short-term factor, and a long-term factor which follows a Brownian motion. The three remaining models, Models 3, 4 and 5, modify the assumption for latent variables, allowing the long-term factor to also follow a mean-reverting process. Models 4 and 5 assume that measurement errors of contracts with different maturities are correlated, based on the belief that the price movement for each contract must be correlated with other available contracts, during the same period within the same market. However, due to an increase in dimensionality in the parameter set, Model 5 attempts at reducing the dimension by estimating volatilities of measurement errors as a parametric function of maturity.

The models' in-sample performances were assessed in Section 3.4.1. Allowing correlations on measurement errors in the model did not substantially improve the model-fit of

the historical price data, due to difference in estimates of volatilities of measurement errors. Assuming independence between measurement errors performed better on calibration of historical price data.

The models' out-of-sample performances were assessed, predicting prices in two different dimensions. Estimating prices for longer-maturity contracts was shown in Section 3.4.2, concluding that models with correlated measurement errors performed better at evaluating prices based on shorter-maturity contracts. Models 4 and 5 may be used to assess the efficiency of longer-maturity contracts based on actively traded shorter-maturity futures contracts. For estimating f-time-steps ahead, shown in Section 3.4.3, Model 3 performed the best, followed by Model 4. Assuming a mean-reverting process for the long-term factor was the key in improving the out-of-sample estimation for EUA futures contracts, as suggested by Benz and Trück [4].

Analysis on residuals was performed in Section 3.5, to validate the normality assumption of measurement errors. The assumption was clearly violated for Model 1, whereas Models 2 and 3, and 5 showed a cluster of observations deviating from the normal distribution, and were significantly different from normality at 5% significance level. Model 4 showed a substantially improved result compared to other models, and validated our key distributional assumption of normality of measurement errors.

Overall, Model 4 performed successfully in all aspects in comparative analysis. This shows that considering correlations between measurement errors of different contracts captures more information about the price movement, than other reduced-form models.

In addition, as there are no additional cost for holding EUAs, theoretically, the link between the spot and the futures prices is mainly explained by interest rate effects only. At this stage, we briefly check the relationship between the interest rate and the futures price of EUA to see whether the changes in interest rates affect the movement of futures price. A 1-year Euro London Inter-Bank Offered Rate (LIBOR) has been used for comparison, with a 1-year EUA futures contracts.

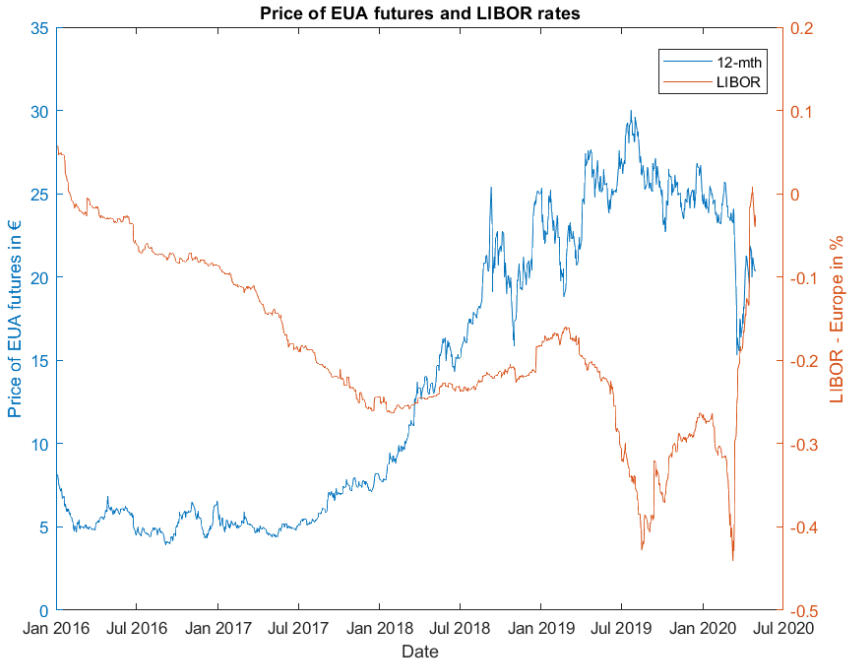

Figure 4.1: Euro LIBOR rates and EUA futures prices, from January 4, 2016 to April 29, 2020

Figure 4.1 clearly shows that there is an inverse relationship between the interest rate and the EUA futures price. For longer term crude oil futures contracts, the relationship between their prices and stochastic interest rates were first studied in Cheng et al. [12]. Hence, it is of our interest to extend our study by modelling stochastic interest rates, as an additional factor to be incorporated into the pricing model to enhance the performance of our best performing multi-factor model. That is, the Model 4 out of five models according to the out-of-sample RMSE and diagnostic checks.

In this thesis, as futures prices have been assumed to be a linear function of the spot price in the state-space model, we may extend for further studies in this area, which include:

1. Using returns of futures prices, a mathematical relationship between principal component factors, which are obtained by probabilistic principal component analysis, and latent state variables can be established.
2. Incorporating stochastic jumps are necessary in cases of sudden changes in business regime or amendments in regulations, as prices dramatically change by sudden shocks in the market. The first two approaches will lead to development of a dynamic carbon emission futures prices forecasting tool.

3. Extending models considered in this thesis by introducing heteroscedasticity, using traded volume to compute volatilities of measurement errors; and
4. Modelling of European call/put options of the stock, by developing the extended Kalman filter algorithm for accommodating non-linearity of the options price and the spot price in the state equation. Application of models to be illustrated using EUA options data.

References

[1] Abadie, L. M. and Chamorro, J. M. (2008), European CO_2 prices and carbon capture investments, *Energy Economics* **30**(6), 2992–3015.

[2] Ainsworth, R. T. (2014), Phishing & VAT fraud in CO_2 permits: DICE in the EU-ETS now; DICE in power tomorrow, *Boston Univ. School of Law, Law and Economics Research Paper* (14-74).

[3] Aspinall, T., Gepp, A., Harris, G., Kelly, S., Southam, C. and Vanstone, B. (2020), Estimation of a term structure model of carbon prices through state space methods: The european union emissions trading scheme, *Accounting & Finance* .

[4] Benz, E. and Trück, S. (2006), CO_2 emission allowances trading in Europe—specifying a new class of assets, *Problems and Perspectives in Management* **4**(3), 30–40.

[5] Benz, E. and Trück, S. (2009), Modeling the price dynamics of CO_2 emission allowances, *Energy Economics* **31**(1), 4–15.

[6] Bierman, G. J. (1973), Fixed interval smoothing with discrete measurements, *International Journal of Control* **18**(1), 65–75.

[7] Binkowski, K., He, P., Kordzakhia, N. and Shevchenko, P. (2019), On the parameter estimation in the Schwartz-Smith's two-factor model, *in Research School on Statistics and Data Science*, Springer, pp. 226-237.

[8] Binkowski, K., Shevchenko, P. and Kordzakhia, N. (2009), Modelling of commodity prices, CSIRO Technical Report CMIS 09/43 .

[9] Black, F. (1976), The pricing of commodity contracts, *Journal of Financial Economics* **3**(1-2), 167–179.

[10] Black, F. and Scholes, M. (1973), The pricing of options and corporate liabilities, *Journal of Political Economy* **81**(3), 637–654.

[11] Carmona, R. and Hinz, J. (2011), Risk-neutral models for emission allowance prices and option valuation, *Management Science* **57**(8), 1453–1468.

[12] Cheng, B., Nikitopoulos, C. S. and Schlögl, E. (2018), Pricing of long-dated commodity derivatives: Do stochastic interest rates matter?, *Journal of Banking & Finance* **95**, 148–166.

[13] Cifuentes, S., Cortazar, G., Ortega, H. and Schwartz, E. S. (2020), Expected prices, futures prices and time-varying risk premiums: The case of copper, *Resources Policy* **69**, 101825.

[14] Convery, F. J. and Redmond, L. (2007), Market and price developments in the European Union emissions trading scheme, *Review of Environmental Economics and Policy* **1**(1), 88–111.

[15] Cortazar, G., Milla, C. and Severino, F. (2008), A multicommodity model of futures prices: Using futures prices of one commodity to estimate the stochastic process of another, *Journal of Futures Markets: Futures, Options, and Other Derivative Products* **28**(6), 537–560.

[16] Cortazar, G., Millard, C., Ortega, H. and Schwartz, E. S. (2019), Commodity price forecasts, futures prices, and pricing models, *Management Science* **65**(9), 4141–4155.

[17] Daskalakis, G., Psychoyios, D. and Markellos, R. N. (2009), Modeling CO_2 emission allowance prices and derivatives: Evidence from the European trading scheme, *Journal of Banking & Finance* **33**(7), 1230–1241.

[18] Delbeke, J., Klaassen, G., Van Ierland, T. and Zapfel, P. (2010), The role of environmental economics in recent policy making at the european commission, *Review of Environmental Economics and Policy* **4**(1), 24–43.

[19] Doha Amendment to the Kyoto Protocol (2012).

[20] Edenhofer, O. (2014), Climate policy: Reforming emissions trading, *Nature Climate Change* **4**(8), 663–664.

[21] Flachsland, C., Pahle, M., Burtraw, D., Edenhofer, O., Elkerbout, M., Fischer, C., Tietjen, O. and Zetterberg, L. (2020), How to avoid history repeating itself: the case for an EU Emissions Trading System (EU ETS) price floor revisited, *Climate Policy* **20**(1), 133–142.

[22] Geman, H. and Nguyen, V.-N. (2005), Soybean inventory and forward curve dynamics, *Management Science* **51**(7), 1076–1091.

[23] Gibson, R. and Schwartz, E. S. (1990), Stochastic convenience yield and the pricing of oil contingent claims, *The Journal of Finance* **45**(3), 959–976.

[24] Green, H., Kordzakhia, N. and Thoplan, R. (2014), Multi-factor statistical modelling of demand and spot price of electricity, *Quality Technology & Quantitative Management* **11**(2), 151–165.

[25] Guo, Z.-Y. (2020), Stochastic multifactor models in risk management of energy futures, *Journal of Futures Markets* .

[26] Gürtler, M., Hibbeln, M. and Vöhringer, C. (2008), Adjusting multi-factor models for Basel II-consistent economic capital, *SSRN Electronic Journal* (1).

[27] Hevia, C., Petrella, I. and Sola, M. (2018), Risk premia and seasonality in commodity futures, *Journal of Applied Econometrics* **33**(6), 853–873.

[28] Hitzemann, S. and Uhrig-Homburg, M. (2019), Empirical performance of reduced-form models for emission permit prices, *Review of Derivatives Research* **22**(3), 389–418.

[29] Hull, J. C. (2003), *Options futures and other derivatives*, Pearson Education India.

[30] Itô, K. (1944), 109. Stochastic Integral, *Proceedings of the Imperial Academy* **20**(8), 519–524.

[31] Kuruppuarachchi, D., Lin, H. and Premachandra, I. (2019), Testing commodity futures market efficiency under time-varying risk premiums and heteroscedastic prices, *Economic Modelling* **77**, 92–112.

[32] Merton, R. C. (1973), Theory of rational option pricing, *The Bell Journal of Economics and Management Science* pp. 141–183.

[33] Napolitano, S., Schreifels, J., Stevens, G., Witt, M., LaCount, M., Forte, R. and Smith, K. (2007), The us acid rain program: key insights from the design, operation, and assessment of a cap-and-trade program, *The Electricity Journal* **20**(7), 47–58.

[34] Occhipinti, Z. and Verona, R. (2020), Kyoto Protocol (KP), *Climate Action* pp. 605–617.

[35] Peters, G. W., Briers, M., Shevchenko, P. and Doucet, A. (2013), Calibration and filtering for multi factor commodity models with seasonality: incorporating panel data from futures contracts, *Methodology and Computing in Applied Probability* **15**(4), 841–874.

[36] Rauch, H. E., Tung, F. and Striebel, C. T. (1965), Maximum likelihood estimates of linear dynamic systems, *AIAA Journal* **3**(8), 1445–1450.

[37] Schwartz, E. and Smith, J. E. (2000), Short-term variations and long-term dynamics in commodity prices, *Management Science* **46**(7), 893–911.

[38] Seifert, J., Uhrig-Homburg, M. and Wagner, M. (2008), Dynamic behavior of CO_2 spot prices, *Journal of Environmental Economics and Management* **56**(2), 180–194.

[39] Shreve, S. E. (2004), Stochastic calculus for Finance II: Continuous-time models, Vol. 11, Springer Science & Business Media.

[40] Sørensen, C. (2002), Modeling seasonality in agricultural commodity futures, *Journal of Futures Markets: Futures, Options, and Other Derivative Products* **22**(5), 393–426.

[41] Trück, S. and Weron, R. (2016), Convenience Yields and Risk Premiums in the EU-ETS—Evidence from the Kyoto Commitment Period, *Journal of Futures Markets* **36**(6), 587–611.

[42] United Nations (1992), United Nations Framework Convention on Climate Change FCCC/INFORMAL/84.

[43] United Nations (1998), Kyoto Protocol to the United Nations Framework Convention on Climate Change.

[44] United Nations Framework Convention on Climate Change (2015), Synthesis report on the aggregate effect of the intended nationally determined contributions. FCC-C/CP/2015/7.

[45] Welch, P. (1967), The use of fast fourier transform for the estimation of power spectra: a method based on time averaging over short, modified periodograms, *IEEE Transactions on Audio and Electroacoustics* **15**(2), 70–73.

[46] Wen, Y. and Kiesel, R. (2016), Pricing options on EU ETS certificates with a time-varying market price of risk model, *Stochastics of Environmental and Financial Economics* pp. 341–360.

A

Appendix A

A.1 Derivation of Expectations and Variances of Latent Factors

Recall, χ_t and ξ_t both follow an Ornstein-Uhlenbeck (O-U) process, as defined in (2.10) and (2.11) under the risk-neutral framework. Using $\{X_t\}_{t\geq 0}$ as a stochastic process which follows an O-U process, the stochastic differential equation is given as

$$dX_t = \alpha(\mu - X_t)dt + \sigma dW_t,$$

where $\alpha > 0$ is the speed of the mean-reversion, $\mu \in \mathbb{R}$ is a long-term mean, $\sigma > 0$ is the instantaneous volatility of X_t, and W_t follows a standard Wiener process.

We let $f(X_t, t) = e^{\alpha t} X_t$. Then, using Itô's Lemma, we have

$$
\begin{aligned}
d\left(f(X_t,t)\right) &= \frac{\partial f(X_t,t)}{\partial t}dt + \frac{\partial f(X_t,t)}{\partial X_t}dX_t + \frac{1}{2}\frac{\partial^2 f(X_t,t)}{\partial X_t^2}dX_t^2, \\
d(e^{\alpha t}X_t) &= \alpha e^{\alpha t}X_t dt + e^{\alpha t}dX_t + 0 \\
&= \alpha e^{\alpha t}X_t dt + e^{\alpha t}\left(\alpha(\mu - X_t)dt + \sigma dW_t\right) \\
&= \alpha e^{\alpha t}X_t dt + \alpha\mu e^{\alpha t}dt - \alpha e^{\alpha t}X_t dt + \sigma e^{\alpha t}dW_t \\
&= \alpha\mu e^{\alpha t}dt + \sigma e^{\alpha t}dW_t
\end{aligned}
$$

and integrating both sides, we have

$$
\begin{aligned}
\int_0^t d(e^{\alpha s}X_s) &= \alpha\mu\int_0^t e^{\alpha s}ds + \sigma\int_0^t e^{\alpha s}dW_s. \\
e^{\alpha t}X_t - X_0 &= \mu(e^{\alpha t} - 1) + \sigma\int_0^t e^{\alpha s}dW_s, \\
X_t &= X_0 e^{-\alpha t} + \mu(1 - e^{-\alpha t}) + \sigma\int_0^t e^{-\alpha(t-s)}dW_s. \qquad \text{(A.1)}
\end{aligned}
$$

From Shreve [39] and Itô [30], as W_t is a martingale, with $W_t - W_s \sim \mathcal{N}(0, t-s)$, $t > s$, for any function $f(t)$ with a continuous derivative on the interval $[0, s]$, the expectation and the variance of Itô integral in (A.1) are

$$
\mathbb{E}\left[\int_0^t f(t)dW_t\right] = 0, \qquad \text{(A.2)}
$$

$$
Var\left[\int_0^t f(t)dW_t\right] = \int_0^t f^2(t)dt, \qquad \text{(A.3)}
$$

Now, for χ_t, factorising the first term of (2.10) and using (A.1), we have

$$
\begin{aligned}
d\chi_t &= \left(-\lambda_\chi - \kappa\chi_t\right)dt + \sigma_\chi dW_t^{\chi*} \\
&= \kappa\left(-\frac{\lambda_\chi}{\kappa} - \chi_t\right)dt + \sigma_\chi dW_t^{\chi*}, \\
\chi_t &= e^{-\kappa t}\chi_0 - \frac{\lambda_\chi}{\kappa}\left(1 - e^{-\kappa t}\right) + \sigma_\chi\int_0^t e^{-\kappa(t-s)}dW_s^{\chi*}.
\end{aligned}
$$

and similarly, for ξ_t, we have

$$
\begin{aligned}
d\xi_t &= \left(\mu_\xi - \lambda_\xi - \gamma\xi_t\right)dt + \sigma_\xi dW_t^{\xi*} \\
&= \gamma\left(\frac{\mu_\xi - \lambda_\xi}{\gamma} - \xi_t\right)dt + \sigma_\xi dW_t^{\xi*}, \\
\xi_t &= e^{-\gamma t}\xi_0 + \frac{\mu_\xi - \lambda_\xi}{\gamma}\left(1 - e^{-\gamma t}\right) + \sigma_\xi\int_0^t e^{-\gamma(t-s)}dW_s^{\xi*}.
\end{aligned}
$$

Hence, as χ_t and ξ_t were assumed to follow a joint bivariate normal distribution, using (A.2) and (A.3),

$$\mathbb{E}^*\left[(\chi_t, \xi_t)\right] = \left(e^{-\kappa t}\chi_0 - \frac{\lambda_\chi}{\kappa}\left(1 - e^{-\kappa t}\right), e^{-\gamma t}\xi_0 + \frac{\mu_\xi - \lambda_\xi}{\gamma}\left(1 - e^{-\gamma t}\right)\right), \tag{A.4}$$

$$\begin{aligned} Var^*\left[\chi_t\right] &= Var\left[\sigma_\chi \int_0^t e^{-\kappa(t-s)} dW_s^{\chi *}\right] \\ &= \sigma_\chi^2 Var\left[\int_0^t e^{-\kappa(t-s)} dW_s^{\chi *}\right] \\ &= \sigma_\chi^2 \int_0^t e^{-2\kappa(t-s)} ds = \frac{1 - e^{-2\kappa t}}{2\kappa}\sigma_\chi^2. \end{aligned} \tag{A.5}$$

and similarly, for ξ_t, the variance of ξ_t is

$$Var^*\left[\xi_t\right] = \frac{1 - e^{-2\gamma t}}{2\gamma}\sigma_\xi^2. \tag{A.6}$$

Lastly, with $\mathbb{E}\left[dW_s^{\chi *} dW_s^{\xi *}\right] = \rho_{\chi\xi} ds$,

$$\begin{aligned} Cov^*\left[(\chi_t, \xi_t)\right] &= \mathbb{E}\left[\left\{\chi_t - \mathbb{E}(\chi_t)\right\}\left\{\xi_t - \mathbb{E}(\xi_t)\right\}\right], \\ &= \mathbb{E}\left[\sigma_\chi \int_0^t e^{-\kappa(t-s)} dW_s^{\chi *} \times \sigma_\xi \int_0^t e^{-\gamma(t-s)} dW_s^{\xi *}\right], \\ &= \mathbb{E}\left[\sigma_\chi \sigma_\xi \rho_{\chi\xi} \int_0^t e^{-(\kappa+\gamma)(t-s)} ds\right], \\ &= \frac{1 - e^{-(\kappa+\gamma)t}}{\kappa + \gamma}\sigma_\chi \sigma_\xi \rho_{\chi\xi}, \end{aligned} \tag{A.7}$$

as shown in (2.12) and (2.13).

Now, to derive the futures price at time t, which matures at time T, integrals shown above need to be evaluated from time t to T, as we evaluate the spot price at time T, conditional on all information up to time t, as shown in (2.17), where

$$F_{t,T} = \mathbb{E}^*\left[S_T | \Im_t\right].$$

This leads (A.1) to becomes

$$X_T = X_t e^{-\alpha(T-t)} + \mu\left(1 - e^{-\alpha(T-t)}\right) + \sigma \int_t^T e^{-\alpha(T-s)} dW_s,$$

and for χ_T and ξ_T, conditional on $\Im_t$, we obtain

$$\chi_T = e^{-\kappa(T-t)}\chi_t - \frac{\lambda_\chi}{\kappa}\left(1 - e^{-\kappa(T-t)}\right) + \sigma_\chi \int_t^T e^{-\kappa(T-s)} dW_s^{\chi *}, \tag{A.8}$$

$$\xi_T = e^{-\gamma(T-t)}\xi_t + \frac{\mu_\xi - \lambda_\xi}{\gamma}\left(1 - e^{-\gamma(T-t)}\right) + \sigma_\xi \int_t^T e^{-\gamma(T-s)} dW_s^{\xi *}. \tag{A.9}$$

Based on (A.8) and (A.9), expectation and the variance of the joint distribution of χ_T and ξ_T, conditional on $\mathfrak{I}_t$ are

$$\mathbb{E}^*\left[(\chi_T,\xi_T)\,|\mathfrak{I}_t\right]=\left(e^{-\kappa(T-t)}\chi_t-\frac{\lambda_\chi}{\kappa}\left(1-e^{-\kappa(T-t)}\right),e^{-\gamma(T-t)}\xi_t+\frac{\mu_\xi-\lambda_\xi}{\gamma}\left(1-e^{-\gamma(T-t)}\right)\right),$$

$$Cov^*\left[(\chi_T,\xi_T)\,|\mathfrak{I}_t\right]=\begin{pmatrix}\frac{1-e^{-2\kappa(T-t)}}{2\kappa}\sigma_\chi^2 & \frac{1-e^{-(\kappa+\gamma)(T-t)}}{\kappa+\gamma}\sigma_\chi\sigma_\xi\rho_{\chi\xi}\\ \frac{1-e^{-(\kappa+\gamma)(T-t)}}{\kappa+\gamma}\sigma_\chi\sigma_\xi\rho_{\chi\xi} & \frac{1-e^{-2\gamma(T-t)}}{2\gamma}\sigma_\xi^2\end{pmatrix}.$$

Note that properties of Itô integral in (A.2) and (A.3) also holds on the interval $[t,T]$, and hence, expectations, variances and the covariance of two factors are derived using the similar approach as (A.4) - (A.7). Now, by (2.1) and (2.16), the futures price at time t is

$$\begin{aligned}\ln F_{t,T}&=\ln\left(\mathbb{E}^*\left[S_T|\mathfrak{I}_t\right]\right)\\&=\mathbb{E}^*\left[\ln\left(S_T|\mathfrak{I}_t\right)\right]+\frac{1}{2}Var^*\left[\ln\left(S_T|\mathfrak{I}_t\right)\right]\\&=\mathbb{E}^*\left[\left(\chi_T+\xi_T+g(T)\right)|\mathfrak{I}_t\right]+\frac{1}{2}Var^*\left[\left(\chi_T+\xi_T+g(T)\right)|\mathfrak{I}_t\right]\\&=e^{-\kappa(T-t)}\chi_t-\frac{\lambda_\chi}{\kappa}\left(1-e^{-\kappa(T-t)}\right)+e^{-\gamma(T-t)}\xi_t+\frac{\mu_\xi-\lambda_\xi}{\gamma}\left(1-e^{-\gamma(T-t)}\right)\\&+\frac{1}{2}\left(\frac{1-e^{-2\kappa(T-t)}}{2\kappa}\sigma_\chi^2+2\frac{1-e^{-(\kappa+\gamma)(T-t)}}{\kappa+\gamma}\sigma_\chi\sigma_\xi\rho_{\chi\xi}+\frac{1-e^{-2\gamma(T-t)}}{2\gamma}\sigma_\xi^2\right)+g(T)\\&=e^{-\kappa(T-t)}\chi_t+e^{-\gamma(T-t)}\xi_t+A(T-t)+g(T),\end{aligned}$$

where

$$\begin{aligned}A(T-t)=&-\frac{\lambda_\chi}{\kappa}\left(1-e^{-\kappa(T-t)}\right)+\frac{\mu_\xi-\lambda_\xi}{\gamma}\left(1-e^{-\gamma(T-t)}\right)\\&+\frac{1}{2}\left(\frac{1-e^{-2\kappa(T-t)}}{2\kappa}\sigma_\chi^2+2\frac{1-e^{-(\kappa+\gamma)(T-t)}}{\kappa+\gamma}\sigma_\chi\sigma_\xi\rho_{\chi\xi}+\frac{1-e^{-2\gamma(T-t)}}{2\gamma}\sigma_\xi^2\right).\end{aligned}$$

as shown in (2.18) and (2.19).

B

Appendix B

B.1 MATLAB Code Used for this Project

The code used for simulation of futures prices, estimation of state variables, and estimation of parameters are presented in this appendix, and are also available here[1]. Brief descriptions on each code are provided in this appendix, and further details are available within each code.

B.1.1 Simulation_Study.m

This code illustrates a simple simulation study, using simulated data set based on the user's choice of the model and inputs for each parameter. All models described in Chapter 2 can be run in this file. The code also includes the process of grid search, performing estimation for every possible set of parameters based on the number of grid points, and the process for computing standard errors of parameter estimates, using bootstrapping approach. `fmincon` is used to minimise the negative log-likelihood function.

[1]Codes are available at https://github.com/Junee1992/EUA_Futures_Pricing

B.1.2 simulatePrice.m

This code simulates futures prices, for N contracts at n time points. The user needs to refer to this code for simulating data using input parameters and model type of his/her choice.

B.1.3 KFS.m

This code runs the Kalman filter and the Kalman smoother algorithm, to estimate latent variables, and hence, calculates the log-likelihood function.